scientific reports

Check for updates

OPEN

Multi-objective energy management in a renewable and EV-integrated microgrid using an iterative map-based self-adaptive crystal structure algorithm

Arul Rajagopalan[1]✉, Karthik Nagarajan[2], Mohit Bajaj[3,4,5]✉, Sowmmiya Uthayakumar[6], Lukas Prokop[7] & Vojtech Blazek[7]

The use of plug-in hybrid electric vehicles (PHEVs) provides a way to address energy and environmental issues. Integrating a large number of PHEVs with advanced control and storage capabilities can enhance the flexibility of the distribution grid. This study proposes an innovative energy management strategy (EMS) using an Iterative map-based self-adaptive crystal structure algorithm (SaCryStAl) specifically designed for microgrids with renewable energy sources (RESs) and PHEVs. The goal is to optimize multi-objective scheduling for a microgrid with wind turbines, micro-turbines, fuel cells, solar photovoltaic systems, and batteries to balance power and store excess energy. The aim is to minimize microgrid operating costs while considering environmental impacts. The optimization problem is framed as a multi-objective problem with nonlinear constraints, using fuzzy logic to aid decision-making. In the first scenario, the microgrid is optimized with all RESs installed within predetermined boundaries, in addition to grid connection. In the second scenario, the microgrid operates with a wind turbine at rated power. The third case study involves integrating plug-in hybrid electric vehicles (PHEVs) into the microgrid in three charging modes: coordinated, smart, and uncoordinated, utilizing standard and rated RES power. The SaCryStAl algorithm showed superior performance in operation cost, emissions, and execution time compared to traditional CryStAl and other recent optimization methods. The proposed SaCryStAl algorithm achieved optimal solutions in the first scenario for cost and emissions at 177.29 €ct and 469.92 kg, respectively, within a reasonable time frame. In the second scenario, it yielded optimal cost and emissions values of 112.02 €ct and 196.15 kg, respectively. Lastly, in the third scenario, the SaCryStAl algorithm achieves optimal cost values of 319.9301 €ct, 160.9827 €ct and 128.2815 €ct for uncoordinated charging, coordinated charging and smart charging modes respectively. Optimization results reveal that the proposed SaCryStAl outperformed other evolutionary optimization algorithms, such as differential evolution, CryStAl, Grey Wolf Optimizer, particle swarm optimization, and genetic algorithm, as confirmed through test cases.

[1]Centre for Smart Grid Technologies, School of Electrical Engineering, Vellore Institute of Technology, Chennai, Tamilnadu 600 127, India. [2]Department of Electrical and Electronics Engineering, Hindustan Institute of Technology & Science, Chennai, Tamilnadu 603 103, India. [3]Electrical Engineering Department, Graphic Era (Deemed to Be University), Dehradun 248002, India. [4]Hourani Center for Applied Scientific Research, Al-Ahliyya Amman University, Amman, Jordan. [5]Graphic Era Hill University, Dehradun 248002, India. [6]Department of Electrical Engineering, SRM Institute of Science and Technology, Kattankulathur, Tamilnadu 603203, India. [7]ENET Centre, VSB—Technical University of Ostrava, 708 00 Ostrava, Czech Republic. ✉email: arulphd@yahoo.co.in; thebestbajaj@gmail.com

Keywords Energy management, Iterative map-based self-adaptive crystal structure algorithm, Electric vehicles, Renewable energy sources, Microgrid, Optimal scheduling, Wind power, Solar photovoltaic

Abbreviations

AER	All-electric range
ASAPSO	Adaptive simulated annealing particle swarm optimization algorithm
BES	Bald eagle search
BESS	Battery energy storage system
BS	Battery storage
BWO	Beluga whale optimization
CBOA	Chef-based optimization algorithm
CHP	Combined heat power
CO_2	Carbon dioxide
DERs	Distributed energy resources
DGs	Distributed generators
DO	Dandelion optimizer
DR	Demand response
DRP	Demand response program
EMS	Energy management strategy
EV	Electric vehicle
FC	Fuel cell
FSAPSO	Fuzzy self-adaptive PSO
GA	Genetic algorithm
GSA-PS	Gravitational search and pattern search
GWO	Grey wolf optimizer
HRES	Hybrid renewable energy system
HS	Heat storage
KH	Krill herd algorithm
LV	Low voltage
MDP	Markov decision process
MG	Microgrid
MGCC	Microgrid central controller
MGO	Mountain gazelle optimizer
MGT	Micro gas turbine
MPC	Model predictive control
MT	Microturbine
MV	Medium voltage
NA	Not available
Nox	Nitrogen dioxide
OGGWO	Oppositional gradient-based grey wolf optimizer
PAFC	Phosphoric acid fuel cell
PDF	Probability density function
PEV	Plug-in electric vehicles
PHEV	Plug-in hybrid electric vehicle
PLR	Peak load reduction
PSO	Particle swarm optimization
PV	Photovoltaic
RES	Renewable energy sources
RUN	Runge Kutta optimization
SaCryStAl	Self-adaptive crystal structure algorithm
SO_2	Sulfur dioxide
SOC	State of charge
WOA	Whale optimization algorithm
WT	Wind turbine

List of symbols

N	Population size
N	Maximum no. of iterations
h	Total number of hours
N_{DG}	Total number of distributing generation units
N_{ST}	Total number of storage units
N_{KL}	Total number of load levels
$U_i(h)$	Status of unit i at hour h
$P_{DGi}(h)$	Active power output of ith distributed generating unit at hour h
$P_{STj}(h)$	Active power output of jth storage unit at hour h
$P_{GR}(h)$	Active power exchanged with the grid through buying or selling at hour hr
$B_{DGi}(h)$	The bid of the ith distributed generation (DG) source during hour h

$B_{STj}(h)$	The bid of the jth storage option during hour h
$B_{GR}(h)$	The bid of grid during hour h
S_{DGi}	Costs associated with starting up or shutting down the ith distributed generation (DG) unit
S_{STj}	Costs associated with starting up or shutting down the jth storage unit
$E_{DGi}(h)$	Emission in kg/MWh for ith distributed generation (DG) unit during hour h
$E_{STj}(h)$	Emission in kg/MWh for jth storage unit during hour h
$E_{GRD}(h)$	Emission in kg/MWh for grid during hour h
$CO_{2_{DG_i}}(h)$	Carbon dioxide emissions from the ith distributed generation (DG) unit during hour h
$SO_{2_{DG_i}}(h)$	Sulphur dioxide emissions from the ith distributed generation (DG) unit during hour h
$NO_{X_{DG_i}}(h)$	Nitrogen oxide emissions from the ith distributed generation (DG) unit during hour h
$CO_{2_{ST_j}}(h)$	Carbon dioxide emissions from the jth storage unit during hour h
$SO_{2_{ST_j}}(h)$	Sulphur dioxide emissions from the jth storage unit during hour h
$NO_{X_{ST_j}}(h)$	Nitrogen oxide emissions from the jth storage unit during hour h
$CO_{2_{GRD}}(h)$	Carbon dioxide emissions from the grid during hour h
$SO_{2_{GRD}}(h)$	Sulphur dioxide emissions from the grid during hour h
$NO_{X_{GRD}}(h)$	Nitrogen oxide emissions from the grid during hour h
P_{LLk}	The quantity of the kth load level
N_{KL}	Total number of load levels
$P_{DG,min}(h)$	Minimum active power generation of ith DG during hour h
$P_{ST,min}(h)$	Minimum active power generation of jth storage unit during hour h
$P_{GR,min}(h)$	Minimum active power generation of grid during hour h
$P_{DG,max}(h)$	Maximum active power generation of ith DG during hour h
$P_{ST,max}(h)$	Maximum active power generation of jth storage unit during hour h
$P_{GR,max}(h)$	Maximum active power generation of grid during hour h
$E_b(h)$	Energy stored in the battery at time h
P_{ch}/P_{disch}	Rate of charge/discharge allowed over a specific timeframe.
ξ_{ch}/ξ_{disch}	Battery efficiency in the process of charging and discharging.
E_b^{min}/E_b^{max}	Limits for the storage capacity of the battery, both minimum and maximum.
$P_{ch,max}/P_{disch,max}$	The highest permissible charge/discharge rate within each time segment, represented as the inertia weight parameter
R_{up}^i	Ramp-up of the ith DG output power
R_{down}^i	Ramp-down of the ith DG output power
Δh	Time step
w	Weighting factor
ρ	Price penalty factor

Microgrids have become a cutting-edge method for tackling the challenges of contemporary energy systems, providing targeted and flexible capabilities for generating, distributing, and managing energy[1,2]. Microgrids, in contrast to conventional centralized grids, are decentralized networks capable of functioning alone or in tandem with the primary grid, offering enhanced resilience, reliability, and efficiency[3,4]. The incorporation of renewable energy sources (RESs), such as solar photovoltaics (PV) and wind turbines (WT), has played a crucial role in the advancement of microgrids[5,6]. Renewable energy sources provide environmentally friendly and sustainable methods of generating energy, hence decreasing dependence on fossil fuels and minimizing the release of greenhouse gases[7]. Furthermore, advancements in energy storage technologies, such as lithium-ion batteries and pumped hydro storage, have significantly enhanced the capacity of microgrids to store excess energy for subsequent use[8,9]. This advancement has led to a more stable power grid and improved integration of intermittent renewable sources[10,11]. The emergence of microgrid technology has paralleled the growing adoption of Plug-In Hybrid Electric Vehicles (PHEVs), presenting both opportunities and challenges in energy management[12,13]. PHEVs serve as both efficient and environmentally friendly modes of transportation, while also serving as mobile energy storage units[14,15]. When incorporated into microgrid operations, plug-in hybrid electric vehicles can actively engage in demand response programs, offer assistance to the grid, and function as alternative power sources in times of emergencies[16,17]. Addressing multi-objective energy management within a microgrid incorporating plug-in electric vehicles (PEVs) represents a crucial and intricate challenge within the realm of energy systems[18,19]. A microgrid is defined as a localized aggregation of electrical loads and distributed energy resources capable of functioning either in a grid-connected or standalone capacity[20–22]. PEVs are becoming increasingly popular as a means of reducing carbon emissions and dependency on fossil fuels[23]. The integration of PEVs into a microgrid creates a new set of challenges and opportunities for energy management[24,25]. PEVs offer the advantage of serving as mobile energy storage units, contributing flexibility and resilience to the microgrid[26]. However, the charging and discharging of PEVs require careful management to fulfill the energy demands of the microgrid while also addressing the requirements of individual PEV owners[27,28]. Multi-objective energy management in a microgrid incorporating PEVs entails the optimization of multiple competing objectives, including minimizing energy expenses, mitigating greenhouse gas emissions, and guaranteeing a dependable and resilient power provision[29–31]. This problem requires sophisticated algorithms and models that can handle the complexity and uncertainty of energy systems. Overall, multi-objective energy management in a microgrid with the integration of PEVs is an important and challenging problem that requires interdisciplinary research and collaboration between experts

in energy systems, optimization, and control theory[32–36]. Its successful implementation can lead to significant benefits, including reduced energy costs, increased energy efficiency, and reduced carbon emissions[37,38].

In[39], a multi-objective economic dispatch model for microgrids incorporating electric vehicles and transferable loads was implemented. Simulation was carried out on four different case studies. The objective functions under consideration included the operational cost of the microgrid, the utilization rate of photovoltaic energy, and the power fluctuation between the microgrid and the utility[40]. A two-stage optimization strategy was implemented to perform the environmental and economic scheduling of microgrid with the integration of electric vehicles[41]. In our previous study[42], we conducted multi-objective energy management in a microgrid integrating plug-in electric vehicles. The model suggested provided a state of charge curve for microgrids, considering the state of charge limits of plug-in electric vehicle batteries to prevent overcharging and over-discharging. Additionally, an enhanced grey wolf algorithm was proposed to address the multi-objective energy management problem. Moreover, in[43], an adaptive simulated annealing particle swarm optimization algorithm (ASAPSO) was introduced for the multi-objective optimal scheduling of microgrids incorporating electric vehicles. The objective functions considered were operational cost and emissions. To strike a better balance between these objectives, coordination of renewable energy consumption and load management was achieved using the linear weighting method, grounded on a two-player zero-sum game. Microgrid energy management strategies with peak load reduction (PLR)-based demand response program was proposed to lower end-user energy costs and lower the peak load demand on the power grid[44]. The optimal management of a microgrid equipped with renewable energy sources and electric vehicles (EVs) alongside responsive loads has been undertaken to achieve cost savings and emissions reduction[45]. To address uncertainties stemming from wind turbine (WT) and photovoltaic (PV) power generation, a demand response program (DRP) was devised to manage required grid reserves. Furthermore, in[46], an optimal microgrid operation considering charging patterns for plug-in hybrid electric vehicles (PHEVs) was proposed. To regulate the charging and discharging processes of PHEVs within the microgrid, along with responsive loads, a smart charging approach was recommended[46]. The study in[47] delved into the stochastic operation planning of a microgrid (MG) incorporating Battery Energy Storage System (BESS), renewable energies, and non-renewable energy sources. They devised a stochastic optimization model with a sole objective and proposed employing a hybrid approach combining the whale optimization algorithm with the pattern search algorithm to tackle the optimization challenge. An ideal energy management system for microgrids, incorporating distributed generation and electric vehicles, was proposed in[48], aiming to reduce operational expenses and environmental pollutants. The optimization approach accounts for the performance of electric vehicles in both petrol and electric modes. In another study[49], a scenario-based stochastic management approach is utilized to achieve the optimal operation of a multi-carrier microgrid (MG). This microgrid incorporates various components such as a wind turbine, photovoltaic panel, fuel cell, microturbine, boiler, combined heat and power unit, along with electrical, thermal, and hydrogen loads, as well as storage facilities for electrical energy, hydrogen, and thermal energy. To further reduce overall running costs, a novel approach for scheduling electric vehicles and battery storage in tandem while considering the demand response program (DRP) is proposed in[50]. Additionally, the impact of DRP collaboration and optimal scheduling of electric vehicles and energy storage systems on operational expenses, power transactions with the upstream grid, hourly distributed energy resources, and system technical parameters is explored. Finally, in[51], a two-stage energy management framework employing stochastic chance constraint model predictive control (MPC) is introduced to solve the microgrid energy management problem with the integration of electric vehicles. The framework adopts a mixed-stage optimization approach, gradually optimizing the problem across various time scales. A detailed investigation into energy management systems (EMS) for microgrids was carried out, emphasizing EMS components and the optimization methodologies integrated into the EMS framework. Extensive literature review on microgrid energy management systems (EMS) was performed, categorizing them according to four criteria: the optimization methods employed, the grid type under consideration, the microgrid's operational mode (connected to the main grid or operating independently), and the software/solvers used as a basis for addressing EMS challenges[52]. An oppositional gradient-based grey wolf optimizer (OGGWO) was proposed to implement the multi-objective optimal scheduling of a microgrid[53]. Table 1 presents an overview of the research contributions in microgrid energy management covering objective functions, optimization methods, test system components, and notable remarks. Since its inception, the crystal structure algorithm has gained widespread popularity due to its remarkable adaptability, simple structure, and lack of predefined parameters. Despite CryStAl's superior performance in several areas, the crystal structure algorithm still has certain flaws. There is not enough exploration since CryStAl is sensitive to local extremes during iteration. To address the limitations of the crystal structure algorithm, we propose the Iterative Map Self-Adaptive Crystal Structure Algorithm (SaCryStAl). The efficacy of the proposed optimization technique was examined across three distinct scenarios to assess its performance.

The contribution to the knowledge section of this paper lies in several key areas. Firstly, we introduce a novel energy management technique tailored specifically for microgrids (MGs) integrated with renewable energy sources (RESs) and Plug-In Hybrid Electric Vehicles (PHEVs). This technique utilizes the SaCryStAl algorithm, which efficiently distributes energy among various units within the grid-connected MG. Secondly we address the dual objectives of minimizing MG operating costs and reducing pollutant emissions, a critical consideration in contemporary energy systems. By formulating an objective function that accounts for both economic and environmental factors, we provide a comprehensive framework for optimizing MG operation. Thirdly, we compare the performance of our proposed algorithm with existing evolutionary optimization approaches, demonstrating its superiority in terms of stability, convergence, and performance. Additionally, we present a true collection of Pareto-optimal solutions, offering system operators a range of options to tailor power dispatch strategies according to their economic and environmental objectives. Lastly, our study highlights the impact of widespread PHEV and RES adoption on grid functioning, underscoring the need for advanced optimization techniques in managing these complex systems. Overall, our contributions advance the field of sustainable energy

References	Year	Components of test system used	Objective functions	Methodology	Remarks
[54]	2024	WT, PV, battery, MT, diesel generator, FC	Operation cost	Intelligent golden jackal optimization	Integration of electric vehicle is not considered
[55]	2023	PV, battery, MT, thermal generator, CHP	Operation cost, emission	Epsilon constraint algorithm	Integration of WT and FC not considered
[56]	2024	WT, PV, battery, MT, diesel generator, FC	Operation cost, emission	Manta ray foraging optimization	Analysis of environmental pollution is ignored. Multi-objective optimization not implemented
[57]	2023	CES, EES, CAES, EHP, AC, heat pump	Operation cost, emission	Blue whale optimization algorithm	Integration of WT, PV, and MT not considered. Different charging modes of EV not analyzed
[58]	2023	PV, WT, battery	MG and EV cost	Enhanced variant multi-objective particle swarm optimization algorithm	Analysis of environmental pollution is ignored
[59]	2023	CHP, gas boiler, WT, PV, HS, BS	Operating cost of multi-microgrid, profit of the distribution company	Mixed-integer linear programming, ε-constraint approach, mixed-integer nonlinear programming	Analysis of environmental pollution is ignored
[60]	2023	WT, PV, battery, MT, diesel generator, FC and grid	Operation cost, emission	Improved shuffled frog leaping algorithm	Different charging modes of EV not analyzed
[61]	2023	thermal generators, battery and grid	operation cost, emission	efficient black widow optimization algorithm,	Integration of renewable energy sources is ignored
[62]	2023	PV, diesel generator, grid and battery	Energy consumption, life cycle of battery, practicality of the renewable energy usage	Extended optimal ε-variable technique	Analysis of operating cost and emission is ignored
[63]	2024	Battery, supercapacitor	Battery capacity loss, state of charge	NSGA-III,	Integration of renewable energy sources is ignored
[64]	2023	WT, MT, PV, FC and battery	Generation cost, penalty cost of frequency overrun	Back Propagation neural network	Analysis of environmental pollution is ignored
[65]	2023	PV, WT, CHP, boiler, battery	Operation cost, emission	Lexicography-compromised programming	Integration of MT and FC is ignored
[66]	2022	WT, PV	Voltage deviation, energy not supplied, overall annual cost of energy in a microgrid	Jellyfish search optimizer	Integration of MT and FC is ignored
[67]	2024	PV, battery	Electricity consumption costs, variability in grid-side energy supply	Multi-objective particle swarm algorithm	Analysis of environmental pollution is ignored
[68]	2024	WT, PV, diesel generator, MGT, battery	Operation cost, emission	Improved PSO algorithm	Integration with EV is ignored
[69]	2023	PV, WT, battery	Operating cost, voltage deviation, active power loss	Wavelet neural network	Analysis of environmental pollution is ignored
[70]	2023	WT, PV	Operating cost, rate of renewable energy, cost of the distribution network operators, cost of electric vehicle users, profit of microgrid operators	Improved PSO algorithm	Analysis of environmental pollution is ignored. Integration of MT and FC is ignored
[71]	2024	WT, PV, battery and grid	Operation cost, emission, voltage deviation, active power loss	Multi-objective artificial vultures optimization algorithm	Integration of MT and FC is ignored
[72]	2023	WT, PV, battery	Operating cost	PSO	Analysis of environmental pollution is ignored. Integration of MT and FC is ignored
[73]	2023	WT, PV, battery	Cost of electric vehicle aggregator	Twin delayed deep deterministic policy gradient algorithm	Analysis of environmental pollution is ignored. Integration of MT and FC is ignored

Table 1. Exploring optimization strategies for energy management in microgrid: a review.

management by providing practical insights and effective solutions for optimizing MG operation in the context of evolving energy landscapes.

The primary contributions of this paper can be outlined as follows:

- Presenting a multi-objective framework for the short-term scheduling of a microgrid (MG) incorporating a plug-in hybrid electric vehicle (PHEV), with cost and emissions as dual objective functions.
- Incorporating the proposed SaCryStAl optimization technique to simultaneously minimize costs and emissions, generate Pareto optimal solutions, and determine the optimal compromise solution using a fuzzy satisfaction method.
- The proposed SaCryStAl is investigated on three different scenarios including the operation of PHEVs' in three different modes.
- The proposed SaCryStAl algorithm produced exceptional results when compared to recently published publications in terms of cost, emission, and solution time.

The rest of the paper is structured as follows:

In section "Iterative map-based self-adaptive crystal structure algorithm (SaCryStAl)", we delve into the implementation of the proposed Iterative map-based Self-Adaptive Crystal Structure Algorithm (SaCryStAl) to address the multi-objective energy management problem. Section "Modeling of a microgrid test system" is dedicated to the modeling of the microgrid test system under consideration. Section "Problem formulation" outlines the formulation of the multi-objective energy management problem aimed at minimizing operating costs and emissions. In section "Fuzzy logic-based selection of optimal compromise solution", we elaborate on the formulation of fuzzy logic assortment for determining the optimal compromise solution. The concept of microgrid modelling is covered in section "Uncertainty models for wind and solar energy". Lastly, section "Modeling of microgrid" presents a comprehensive demonstration of the superior performance and feasibility of the proposed SaCryStAl algorithm, juxtaposed with other meta-heuristic optimization algorithms such as FSAPSO, KH, PSO, WOA, GA and GWO.

Iterative map-based self-adaptive crystal structure algorithm (SaCryStAl)

Classical crystal structure algorithm (CryStAl)

The mathematical model of CryStAl, which applies the fundamental ideas of crystal formulation with the appropriate adjustments, is described in this part. All possible solutions to the optimization procedure are viewed as individual crystals in the solution space in this model. Initial crystals are generated randomly[74]. The idea of adding a basis to lattice points to create crystals served as the inspiration for the crystal structure algorithm. Siamak Talatahar suggested this crystal structure algorithm in 2021 based on this idea[75].

The initial population is randomly generated within the bounds using Eq. (1).

$$X_{i,j} = L_{i,j} + r * \left(U_{i,j} - L_{i,j}\right), \quad \mathrm{i} = 1, 2, ..., \quad N, \mathrm{j} = 1, 2, ..., \mathrm{m}. \tag{1}$$

where $X_{\mathrm{i,j}}$ is the jth variable in the ith solution vector, where m is the problem's dimension and N is the number of crystals or potential solutions. "r " is a random number between [0, 1], L_j and U_j are the variables, lower and upper bounds. The structure of the initial population matrix is shown in Eq. (2).

$$\mathrm{C} = \begin{bmatrix} C_{i1} \\ C_{i2} \\ \vdots \\ C_{iN} \end{bmatrix} = \begin{bmatrix} x_{1,1} & \cdots & x_{1,m} \\ x_{2,1} & \ldots & x_{2,m} \\ \vdots & \cdots & \vdots \\ x_{N,1} & \ldots & x_{N,m} \end{bmatrix}, \quad \mathrm{i} = 1, 2, \ldots, N \& \mathrm{j} = 1, 2, \ldots, \mathrm{m}. \tag{2}$$

Based on the concept of 'basis' in crystallography, all the crystals at the corners are considered as the main crystals (C_{rM}). The crystal with the best fitness value is taken as C_{rb} and the mean values of randomly-selected crystals are denoted by F_c. The new crystals are generated in the search space by using the following Eqs. (3–6). This process will be repeated for N number of iterations considered.

(i) Simple cubicle:

$$\mathrm{C}_{rN} = \mathrm{C}_{rO} + r\mathrm{C}_{rM} \tag{3}$$

(ii) Cubicle with the best crystals:

$$\mathrm{C}_{rN} = \mathrm{C}_{rO} + r_1\mathrm{C}_{rM} + r_2\mathrm{C}_{rb}, \text{ where } r_1 = (1 - r) \& r_2 = r_1/\mathrm{N} \tag{4}$$

(iii) Cubicle with the mean crystals:

$$\mathrm{C}_{rN} = \mathrm{C}_{rO} + r_1\mathrm{C}_{rM} + r_2F_c \tag{5}$$

(iv) Cubicle with the best and mean crystals:

$$\mathrm{C}_{rN} = \mathrm{C}_{rO} + r_1\mathrm{C}_{rM} + r_2\mathrm{C}_{rb} + r_3F_c, \quad \text{where } r_3 = r_2/\mathrm{N} \tag{6}$$

where, in the four equations above, C_{rN} is the new position, C_{rO} is the old position, and r, r_1, r_2 and r_3 are random numbers related to one another.

Steps involved in the proposed Iterative map-based self-adaptive crystal structure algorithm

Step 1 Generate N number of initial crystals $\left(X_{i,j}\right)$ using the Eq. (1) and find the opposite values for all the crystals $\left(\overline{X}_{ij}\right)$ using the Eq. (7).

$$\overline{X}_{ij} = U_{\mathrm{i}} + L_{\mathrm{i}} - X_{ij}, \qquad \mathrm{i} = 1, 2, \ldots, \mathrm{N} \& \mathrm{j} = 1, 2, \ldots, \mathrm{n} \tag{7}$$

Calculate the fitness function value for all the crystals, arrange them in ascending order, and take the first N as the initial population size.

Step 2 Generate the random (r) value using an iterative map [76] Eq. (8).

$$r_{n+1} = \sin\left(\mathrm{a}/r_n\right) \tag{8}$$

'a' represents a parameter that can be adjusted. Its value ranges from 0 to ɑ. Based on our experience, the optimal value of 'a' is fixed as 0.48 and the starting rand (r_n) value is 0.26.

Step 3 Generate four new crystals using Eqs. (3–6) and find their opposite values using Eq. (7). Select the best crystal out of the eight newly created values and compare its fitness value with the fitness values of the initial population. If the best crystal replaces any one of the worst crystals in the initial population then maintain the r_n values in the Eq. (3). Otherwise, generate a new value r_n using Eq. (8). The detailed working mechanism of the proposed algorithm is given in Fig. 1.

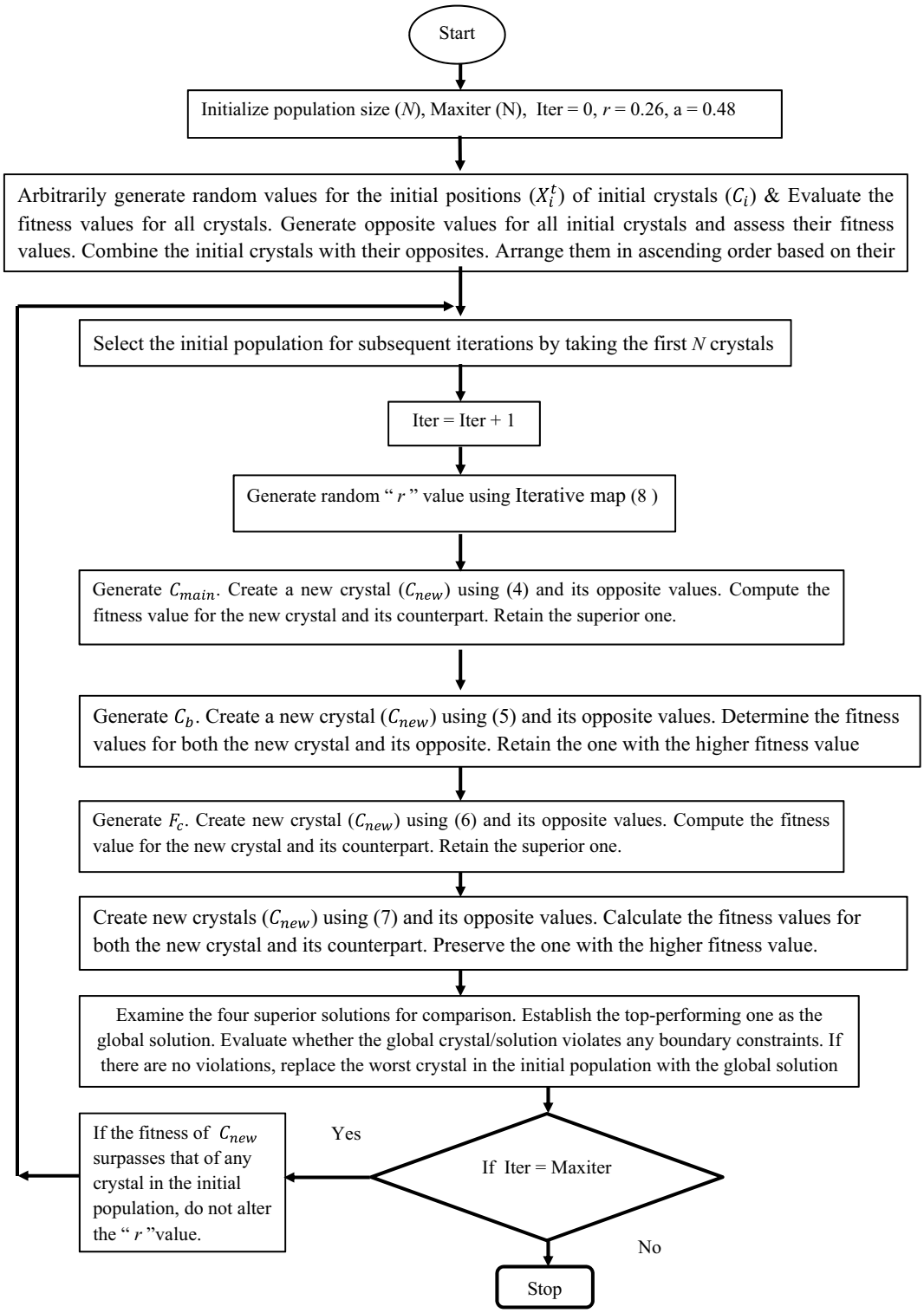

Figure 1. Flowchart outlining the SaCryStAl algorithm.

Pseudo-code of SaCryStAl

Initializing the positions of crystals C_{ij} and $\overline{C}_{ij}$ using (1) & (7).
Calculate the fitness value for all the crystals.
Generate random " r " value using Eq. (8)
while $N < N_{max}$ do.
for (every crystal) do.
Create C_{rM}.
Create new crystals through formula (3) and its opposite value.
Generate C_{rb}.
Construct new crystals through formula (4) and its opposite value.
Create F_c.
Create new crystals through formula (5) and its opposite value.
Create new crystals through formula (6) and its opposite value.
if (all the newly created crystal exceeds the limits) then adjust the location of the new crystal.
end if.
Compute the fitness values for all the newly generated crystals.
Revise the population with the best fitness value.
end for.
$N = N + 1$.
end while.
Display the best crystal.

To assess the efficacy of the suggested algorithm, we select five standard mathematical test functions and proceed with its implementation. The outcomes from our method surpass those of the conventional approach and other methods referenced in Ref.[77], while matching the performance of the ABC method in terms of quality. Table 2 presents the test data from applying the classical and proposed algorithm to benchmark functions.

Modeling of a microgrid test system

This research investigates a grid-connected microgrid (MG) comprising a wind turbine (WT), photovoltaic (PV) array, microturbine (MT), fuel cell (FC), storage battery, plug-in hybrid electric vehicles (PHEVs), and loads, connected to the main grid via a 20 kV/400 V transformer[78,79]. The microgrid configuration under study is adapted from the topology outlined in Ref.[78]. The PHEV represents a unique vehicle with various charging options and a transportation system enabling the use of fossil fuels during extended journeys if the battery's charge depletes[80,81]. Factors such as the state of charge (SOC) of the PHEV's battery, charger size, charging duration, and vehicle volume influence its charging rate[82,83]. Considering the unpredictable charging demands of these vehicles, our research encompasses multiple charging methods—coordinated, uncoordinated, and smart charging—to comprehensively characterize this phenomenon[84,85].

In the initial charging pattern being examined, termed uncoordinated charging, the plug-in hybrid electric vehicles (PHEVs) have the flexibility to connect to the grid for charging at any time they desire[86,87]. These vehicles typically undertake two daily trips, with the first occurring in the morning and the second in the evening as they return home. Upon arriving home at 6:00 PM, it is assumed that the vehicles have the opportunity to connect to the grid for charging purposes. The probability density function (PDF) can be used to develop this[88] as follows:

$$f(t_{start}) = \frac{1}{b-a} a \le t_{start} \le ba = 18,\ b = 19 \tag{9}$$

where a and b represent constants referring to the time.

S.No	Name of the function	Objective function	Characteristics	Dime-nsions	Range	Method	f_{op}	Mean	Std.Dev
1	Sphere	$f_1(x) = \sum_{i=1}^{n} x_i^2$	Unimodal separable	30	[−100,100]	CM	0.00982	0.0693	0.2736
						PM	0	0	0
2	Schwefel 1.2	$f_2(x) = \sum_{i=1}^{n} \left(\sum_{j=1}^{i} x_j \right)^2$	Unimodal non-separable	30	[−100,100]	CM	0.00875	0.0946	0.0438
						PM	0	0	0
3	Rosenbrock	$f_3(x) = \sum_{i=1}^{n-1} \left(100\left(x_{i+1} - x_i^2\right)^2 \right) + (x_i - 1)^2$	Unimodal non-separable	30	[−30,30]	CM	0.00948	1.096897	0.09576
						PM	0	0.0887707	0.077390
4	Quartic	$f_4(x) = \sum_{i=1}^{n} i x_i^4 + \text{random}[0, 1)$	Unimodal separable	30	[−1.28,1.28]	CM	0.00264	0.04858	0.02623
						PM	0	0.030017	0.004868
5	Rastrigin	$f_5(x) = \sum_{i=1}^{n} \left[x_i^2 - 10\cos(2\pi x_i) + 10 \right]$	Multimodal separable	30	[−5.12,5.12]	CM	0.00035	0.000257	0.000537
						PM	0	0	0

Table 2. Exploration of the proposed SaCryStAl algorithm to benchmark test functions. *CM* classical method & *PM* proposed method.

In the coordinated charging pattern, owners of plug-in hybrid electric vehicles (PHEVs) opt to connect their vehicles to the grid during off-peak hours to circumvent peak times and associated high prices. Consequently, they typically initiate charging sessions after 9:00 PM. This preference for off-peak charging is articulated in[88].

$$f(t_{start}) = \frac{1}{b-a} a \leq t_{start} \leq ba = 21,\ b = 24 \tag{10}$$

In a smart charging pattern, PHEVs are connected to the grid when power prices are at their lowest or when energy is abundant[89]. This pattern can be represented using a standard PDF as seen below[88]:

$$f(t_{start}) = \left(\frac{1}{\sigma\sqrt{2\pi}}\right) e^{0.5\left(\frac{t_{start}-\mu}{\sigma}\right)^2} \mu = 1,\ \sigma = 3 \tag{11}$$

where μ and σ represent the standard deviation and mean respectively.

With the use of all-electric range (AER), the SOC of PHEVs during the charging process may be calculated as follows:

$$SOC = \begin{cases} 0m > AER \\ \frac{AER-m}{AER} \times 100m \leq AER \end{cases} \tag{12}$$

Here, m represents the mileage of the PHEV in miles. Our study focuses on the PHEV-20 model, and charger availability data is sourced from[90]. We illustrate the charging process in residential areas using level 1 and level 2 chargers, which are the focus of this research. Level 3 chargers are designated for commercial and public transportation purposes.

Problem formulation

In this study, we introduce a precise mathematical model for short-term energy management aimed at minimizing operating costs and pollution emissions within a microgrid. Achieving optimal performance in a microgrid involves utilizing a multi-objective optimization approach. The key aim of multi-objective energy management in a typical microgrid setting is to identify the best power generation levels and determine the suitable operational states (ON or OFF) for distributed generation units. This process must optimize both the microgrid's operating costs and its net emissions, all while complying with predefined equality and inequality constraints. This study introduces a detailed mathematical model tailored for short-term energy management, aiming to cut costs and reduce emissions within the microgrid.

Objective functions

Optimizing both cost and emissions in a grid-connected microgrid is essential for balancing economic efficiency, environmental sustainability, regulatory compliance, and social responsibility. By targeting these goals simultaneously, microgrid operators can enhance their operations to benefit stakeholders and society at large. This study examines two key objective functions: operational costs and pollution emissions.

Operating cost

Operational costs form a foundational aspect of energy management strategies, significantly influencing their effectiveness and efficiency. These costs play a vital role in ensuring the economic sustainability and viability of microgrid operations[91]. Total operational expenses for the microgrid, calculated in Euro cents (€ct), encompass fuel costs for distributed generation units, startup and shutdown expenses, and costs associated with power exchange between the utility and the microgrid. The aim of managing overall operating costs is to achieve optimal power flow from energy sources to load centers over a given period, while prioritizing cost-effectiveness.

Operational costs contribute to bolstering the resilience and stability of microgrid systems. By accounting for factors such as fuel and maintenance expenses and penalties for deviations from operational constraints, these costs help identify robust energy management strategies that can endure uncertainties and disturbances, ensuring a reliable and continuous power supply[91].

$$\min f_{T.C}(X) = \sum_{h}^{T} \left(TC_{DG}^{h} + TC_{ST}^{h} + TC_{GR}^{h}\right) \tag{13}$$

$$TC_{DG}^{h} = C_{PV}^{h} + C_{WT}^{h} + C_{MT}^{h} + C_{FC}^{h} \tag{14}$$

$$C_{PV}^{h} = U_{PV}(h) \cdot P_{PV}(h) \cdot B_{PV}(h) + S_{PV} \cdot |U_{PV}(h) - U_{PV}(h-1)| \tag{15}$$

$$C_{WT}^{h} = U_{WT}(h) \cdot P_{WT}(h) \cdot B_{WT}(h) + S_{WT} \cdot |U_{WT}(h) - U_{WT}(h-1)| \tag{16}$$

$$C_{MT}^{h} = U_{MT}(h) \cdot P_{MT}(h) \cdot B_{MT}(h) + S_{MT} \cdot |U_{MT}(h) - U_{MT}(h-1)| \tag{17}$$

$$C_{FC}^{h} = U_{FC}(h) \cdot P_{FC}(h) \cdot B_{FC}(h) + S_{FC} \cdot |U_{WT}(h) - U_{FC}(h-1)| \tag{18}$$

$$CT_{ST}^{h} = U_{BT}(h) \cdot P_{BT}(h) \cdot B_{BT}(h) + S_{BT} \cdot |U_{BT}(h) - U_{BT}(h-1)| \tag{19}$$

$$CT_{GR}^{h} = P_{GR}(h) \cdot B_{GR}(h) \tag{20}$$

At hour h, the variables U_{PV}, U_{WT}, U_{MT}, U_{FC}, and U_{BT} represent the operating states of the solar photovoltaic system, wind turbine, microturbine, fuel cell, and battery, respectively. Similarly, the bids for distributed generators (DGs), storage devices, and the grid at hour hr are denoted by B_{PV}, B_{WT}, B_{MT}, B_{FC}, B_{BT} and B_{GR}. The power outputs of the solar photovoltaic, wind turbine, microturbine, fuel cell, and battery unit at time h are represented by $P_{PV}(h)$, $P_{WT}(h)$, $P_{MT}(h)$, $P_{FC}(h)$ and $P_{BT}(h)$ respectively. The start-up and shut-down costs of the solar photovoltaic, wind turbine, microturbine, fuel cell, and battery units are indicated by S_{PV}, S_{WT}, S_{MT}, S_{FC} and S_{BT} respectively. Additionally, $P_{GR}(h)$ denotes the quantity of power traded with the market at hour hr, as referenced in[74,91].

This study focuses on the design variables, which include the generated power outputs and the operating states of the generation units. The decision variables, consisting of the active power of the units and their corresponding states, are represented by the vector X, as defined in[91].

$$X = \left[P_{DG}, P_{ST}, U_{DG}, U_{ST}\right] \tag{21}$$

$$P_{DG} = [P_{DG1}, P_{DG2}, \ldots, P_{DGi}, P_{GRD}] \forall \in N_{DG} \tag{22}$$

$$P_{ST} = \left[P_{ST1}, P_{ST2}, \ldots, P_{STj}\right] \forall \in N_{ST} \tag{23}$$

$$U_{DG} = [U_{DG1}, U_{DG2}, \ldots, U_{DGi}] \tag{24}$$

$$U_{ST} = \left[U_{ST1}, U_{ST2}, \ldots, U_{STj}\right] \tag{25}$$

Here N_{DG} characterizes the number of distributed generators (DGs) installed in the microgrid (MG), whilst N_{ST} signifies the number of storage units.

Objective function for pollution

The objective function for emissions is essential for evaluating the environmental impact of microgrid operations[92]. Microgrids emit pollutants due to various components such as the grid, generation units, and energy storage resources[93]. By quantifying emissions of pollutants such as CO_2, SO_2, and NO_x, this function provides a comprehensive measure of the ecological footprint of energy generation and consumption within the microgrid. This is particularly significant in addressing climate change and mitigating air pollution, as it allows stakeholders to monitor and reduce the environmental effects of energy production[94]. The emissions objective function plays a crucial role in aligning energy management strategies with regulatory standards and sustainability goals. By incorporating emissions considerations into the optimization process, it supports compliance with emissions regulations and fosters proactive environmental stewardship. This helps microgrid operators avoid potential penalties and regulatory challenges while positioning them as leaders in promoting clean energy practices. Additionally, the emissions objective function enhances the overall efficiency and resilience of microgrid systems. By optimizing energy management strategies to minimize emissions while meeting operational needs, it encourages the adoption of cleaner and more sustainable technologies. The mathematical formula for calculating emissions, including nitrogen dioxide (NO_x), carbon dioxide (CO_2), and Sulfur dioxide (SO_2), is presented below[91].

Min

$$\min f_{T.E}(X) = \sum_{h=1}^{T} \left\{ \sum_{i=1}^{N_{DG}} [U_i(h) P_{DGi}(h) E_{DGi}(h)] + \sum_{j=1}^{N_{ST}} \left[U_j(h) P_{STj}(h) E_{STj}(h)\right] + (P_{GR}(h) E_{GR}(h)) \right\} \tag{26}$$

Here $E_{DGi}(h)$, $E_{STj}(h)$, and $E_{GR}(h)$ denote the amount of pollutants from ith distributed generating unit, jth storage unit, and the market, at hour h, in kg/MWh correspondingly.

The emission variables are symbolized as follows[91]:

$$E_{DGi}(h) = \mathrm{CO2}_{DG_i}(h) + \mathrm{SO2}_{DG_i}(h) + \mathrm{NO}_{x_{DG_i}}(h) \tag{27}$$

Here $\mathrm{CO2}_{DG_i}(h)$, $\mathrm{SO2}_{DG_i}(h)$ and $\mathrm{NO}_{x_{DG_i}}(h)$ characterize the emissions of CO_2, SO_2, and NO_x correspondingly from the ith DG sources during the hour h of the day.

$$E_{STj}(h) = \mathrm{CO2}_{ST_i}(h) + \mathrm{SO2}_{ST_i}(h) + \mathrm{NO}_{x_{ST_i}}(h) \tag{28}$$

Here $\mathrm{CO2}_{ST_i}(h)$, $\mathrm{SO2}_{ST_i}(h)$ and $\mathrm{NO}_{x_{ST_i}}(h)$ signify the emissions of CO_2, SO_2, and NO_x correspondingly from the jth storage unit at hour h.

$$E_{GR}(h) = \mathrm{CO2}_{GR}(h) + \mathrm{SO2}_{GR}(h) + \mathrm{NO}_{x_{GR}}(h) \tag{29}$$

Here $CO_{2_{GR}}(h)$, $SO_{2_{GR}}(h)$ and $NO_{x_{GR}}(h)$ represent the emissions of CO_2, SO_2, and NO_x correspondingly from the macro-grid or utility during the hour h of the day.

Constraints and limitations

Load-generation balance

$$\sum_{k=1}^{N_{KL}} P_{LLk}(h) + \sum_{m=1}^{N_{PHEV}} P_{PHEV,m}(h) = \sum_{i=1}^{N_{DG}} [P_{DGi}(h)] + \sum_{j=1}^{N_{ST}} \left[P_{STj}(h)\right] + (P_{GR}(h)) \tag{30}$$

Here, P_{LLk} represents the load magnitude of the kth load, whilst N_{KL} denotes the total number of load levels present within the utility, as defined in Ref.[91].

Generated power

The entire set of units, including the market, storage units, and distributed generators (DG), has defined lower and upper limits that regulate their power generation capacities, as described in Ref.[91]. The output power from the MG components should achieve the following constraints[53].

$$\begin{aligned} P_{DGi,min}(h) \le P_{DGi}(h) \le P_{DGi,max}(h) \\ P_{STj,min}(h) \le P_{STj}(h) \le P_{STj,max}(h) \\ P_{GR,min}(h) \le P_{GR}(h) \le P_{GR,max}(h) \end{aligned} \tag{31}$$

The formula provided in Eq. (9) stipulates that the power generated from distributed generation (DG), battery, and grid sources must fall within their designated minimum and maximum limits, denoted by "min" and "max" respectively.

DGs' ramp rate constraints

This constraint pertains to the adjustment of the output power from distributed generators (DGs), describing the condition as follows[78]:

$$R^i_{down} \cdot \Delta h \le P(h)^i - P(h-1)^i \le R^i_{up} \cdot \Delta h \tag{32}$$

where R^i_{down} and R^i_{up} are the ramp-down and ramp-up of the ith DG output power, respectively, and Δh is the time step in hours.

Battery charging/discharging states

To avoid the damage of the battery, the following constraint should be achieved[78,95]:

$$E_b^{min} \le E_b(h) \le E_b^{max} \tag{33}$$

$$P_{ch}(h) \le P_{ch}^{rated}, P_{disch}(h) \le P_{disch}^{rated} \tag{34}$$

where E_b^{min} represents the minimum stored energy in the battery while E_b^{max} denotes the maximum stored energy, P_{ch}^{rated} is the battery rated charge power, and P_{disch}^{rated} represents the battery rated discharge power during each time interval Δh.

The battery stored energy can be calculated as follows[78]:

$$E_b(h) = E_b(h-1) + \xi_{ch} P_{ch}(h)\Delta h - \frac{1}{\xi_{disch}} P_{disch}(t)\Delta h \tag{35}$$

where ξ_{ch} is the charging efficiency while ξ_{disch} represents the discharging efficiency.

Here $E_b(h)$ and $E_b(h-1)$ represent the energy stored in the battery at hours h and $h-1$, respectively. P_{ch} is the permissible charging rate, while P_{disch} is the permissible discharging rate during a specific time interval (Δh). The battery's charging and discharging efficiency are denoted by ξ_{ch} and ξ_{disch} respectively[96,97].

Formulation of multi-objective energy management problem

The multi-objective energy management problem is formulated as follows:

$$Minimize f_{CE}\left(f_{T.C}, f_{T.E}\right) \tag{36}$$

In this context, $f_{T.C}$ represents the objective function focused on cost minimization, while $f_{T.E}$ is the objective function targeting emissions reduction. By integrating a price penalty factor (ρ), the multi-objective energy management problem can be transformed into a single-objective optimization problem, as shown in Eq. (26). The approach for determining the value of ρ is detailed in[98].

$$Minimize f_{CE} = \sum_{i=1}^{N} \left(\left(w \times f_{T.C} \right) + \left(\rho \times (1 - w) \times f_{T.E} \right) \right) \tag{37}$$

In this context, the weighting factor 'w' signifies the degree of importance assigned to a specific objective function. With 'w' set to 1, the optimization primarily emphasizes the reduction of operational costs. Conversely, assigning 'w' a value of 0 prioritizes the minimization of emissions. In the context of multi-objective energy management, the 'w' value is systematically reduced from 1 to 0, and at each decrement, a compromised solution is generated. Ultimately, the best compromised solution (BCS) is determined using the fuzzy membership approach outlined in section "Fuzzy logic-based selection of optimal compromise solution", where a decrease in 'w' leads to a simultaneous increase in operational costs and a reduction in pollutant emissions.

Fuzzy logic-based selection of optimal compromise solution

Before making a decision, it is crucial to determine the optimal compromise solution from the available set of optimal solutions[99,100]. To identify the best compromise solution, the author employed a fuzzy membership approach[101]. In jth objective function, f_j of individual k is characterized by a membership function μ_j^k due to indefinite characteristic of decision maker's conclusion which is represented as follows[102]:

$$\mu_j^k = \begin{cases} 1 & f_j \le f_j^{min} \\ \frac{f_j^{max} - f_j}{f_j^{max} - f_j^{min}} & f_j^{min} < f_j < f_j^{max} \\ 0 & f_j \ge f_j^{max} \end{cases} \tag{38}$$

where f_j^{max} denote the maximum value of jth fitness function while the latter's minimum value is represented by f_j^{min} in the pool of non-dominated solutions. Here, the normalized membership function μ^k is also determined accordingly for each non-dominated solution k as follows[103]:

$$\mu^k = \frac{\sum_{j=1}^{N} \mu_j^k}{\sum_{k=1}^{r} \sum_{j=1}^{N} \mu_j^k} \tag{39}$$

Here, the overall number of non-dominated solutions is denoted by r. The best compromise solution is composed of maximum value, μ^k.

Uncertainty models for Wind and Solar Energy

Different types of PDFs (Probability Density Function) have been deployed for the characterization of stochastic output power from the RESs. The wind turbine-based power relies upon the speed of the wind. As per the literature[104–106], Weibull PDF forms the basis for wind speed probability.

$$f_{wv}(v) = \left(\frac{\alpha}{\lambda} \right) \left(\frac{v}{\lambda} \right)^{(\alpha - 1)} exp[^{-\left(\frac{v}{\lambda} \right)}]^{\alpha} \quad for \quad 0 < v < \infty \tag{40}$$

Here, the shape parameter of Weibull PDF is denoted by α whereas λ corresponds to the scale of Weibull PDF. These variable values are sourced from the literature[104]. The following Eq. (41) shows the average of Weibull PDF.

$$M_w = \lambda * \Gamma \left(1 + \alpha^{-1} \right) \tag{41}$$

The equation given below (25) describes the Γ function.

$$\Gamma \left(x' \right) = \int_0^{\infty} e^{-t} t^{x'-1} dt \tag{42}$$

The fluctuations that occur in wind speed for the wind farm are shown in Fig. 2. As per the literature[7], both scale and shape parameter values are decided. On the other hand, the PDF parameter values are chosen according to the study conducted earlier[104,107]. The aggregated rated output generated by the wind farm with capacity of 15 MW is achieved by connecting 5 wind generators in the considered microgrid test system. Each individual wind generator has a capacity of 3 MW. The subsequent Eq. (43) describes the power produced by the wind generators that relies upon the speed of the wind.

$$P_{WG} = \begin{matrix} 0 & for \ v \le v_{in} \\ P_{W_r} \left(\frac{v - v_{in}}{v - v_{out}} \right) & for \ v_{in} \le v \le v_r \\ P_{W_r} & for \ v_r \le v \le v_{out} \end{matrix} \tag{43}$$

Here, P_{W_r} corresponds to a single turbine's rated power whereas the cut-in speed is denoted by v_{in}. On the other hand, the cut-out speed is characterized by v_{out} and the rated speed is denoted by v_r. In this research work, various Weibull parameters are considered for the distribution of wind speed in line with literature[104,107]. From the wind generators, rated power is generated within the wind speed range that falls between the cut-in and cut-out thresholds. As per the literature[104,107], the probability of such discrete zones is shown in the Eq. (44).

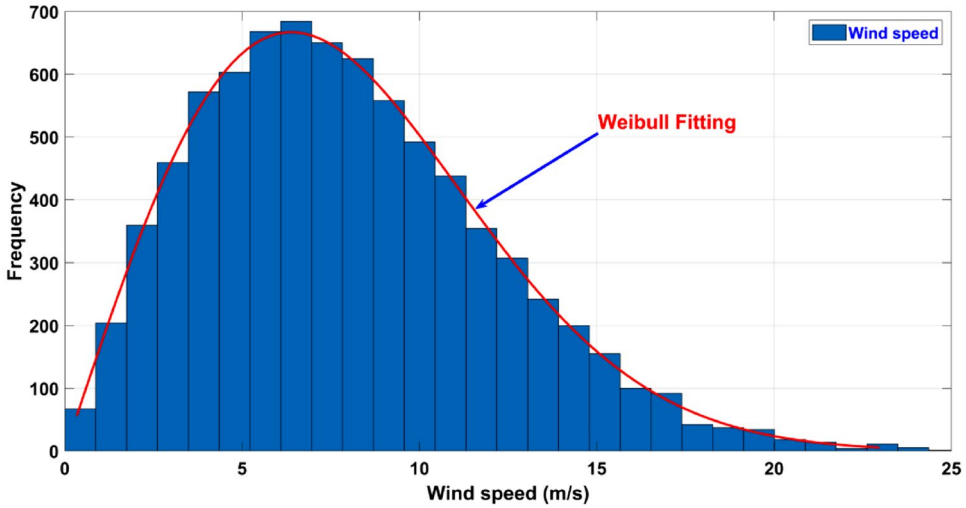

Figure 2. Wind speed variation for wind farm.

$$f_{P_{WG}} = 1 - \exp\left[-\left(\frac{v_{in}}{\lambda}\right)^{\alpha}\right] + \exp\left[-\left(\frac{v_{out}}{\lambda}\right)^{\alpha}\right] \quad for \quad (P_{WG} = 0) \tag{44}$$

$$f_{P_{WG}} = \exp\left[-\left(\frac{v_r}{\lambda}\right)^{\alpha}\right] - \exp\left[-\left(\frac{v_{out}}{\lambda}\right)^{\alpha}\right] \quad for \quad (P_{WG} = P_{WR}) \tag{45}$$

In continuous region, the probability distribution for wind power is as follows.

$$f_{P_{WG}} = \frac{\alpha(v_r - v_{in})}{\lambda^{\alpha} * P_{wr}}\left[v_{in} + \frac{P_{WG}}{P_{wr}}(v_r - v_{in})\right]^{\alpha-1} exp - \left(\frac{(v_{in} + \frac{P_{WG}}{P_{wr}}(v_r - v_{in})}{\lambda}\right)^{\alpha} \tag{46}$$

Likewise, the power generated by solar PV system completely relies upon the solar irradiance (G) that suits the guidelines as per lognormal PDF[104,107]. As per the literature[108], the following equation shows the probability of solar irradiance with mean as well as standard deviation.

$$f_{PV}(G) = \frac{1}{G\sigma\sqrt{2\pi}} \exp\left[-\frac{(\ln x - \mu)^2}{2\sigma^2}\right] \quad for \quad G > 0 \tag{47}$$

The subsequent Eq. (48) yields the mean of lognormal distribution (M_{Lgn})

$$M_{Lgn} = \exp\left(\mu + \frac{\sigma^2}{2}\right) \tag{48}$$

Figure 3 shows the frequency distribution for lognormal fitting and solar irradiance in case of simulating the Monte-Carlo scenario using 8,000 samples. The solar PV output power is expressed herewith.

$$P_{PV}(G) = \begin{matrix} P_{PVr}\left(\frac{G^2}{G_{std}R_C}\right) & for \ 0 \le G \le R_C \\ P_{PVr}\left(\frac{G}{G_{std}}\right) & for \ G \ge R_C \end{matrix} \tag{49}$$

In a standard environmental setting, solar irradiance is denoted as G_{std}, with specific irradiance represented by R_C. For G_{std}, the value assumed is 800 W/m^2, while R_C is set at 120 W/m^2. For the PV module, the rated output power P_{PVr} is specified as 25 MW.

Modeling of microgrid

Utilizing individual distributed generators (DGs) can introduce numerous challenges, highlighting the importance of adopting a system approach. This approach treats generation and associated loads as a subsystem or microgrid[109,110]. By aggregating distributed generators (DGs) within a microgrid and harnessing renewable energies in large quantities, various issues related to economy, technology, and environment can be carefully studied within the target system, enabling informed decisions for improved operational management[111,112]. Furthermore, distributed generation encompasses a diverse array of prime mover technologies, including internal combustion (IC) engines, gas turbines, microturbines, photovoltaic systems, fuel cells, and wind power. These emerging technologies typically exhibit lower emissions and have the potential to achieve lower costs, thus challenging traditional economies of scale[78]. For instance, fuel cells, which generate electricity from hydrogen and oxygen,

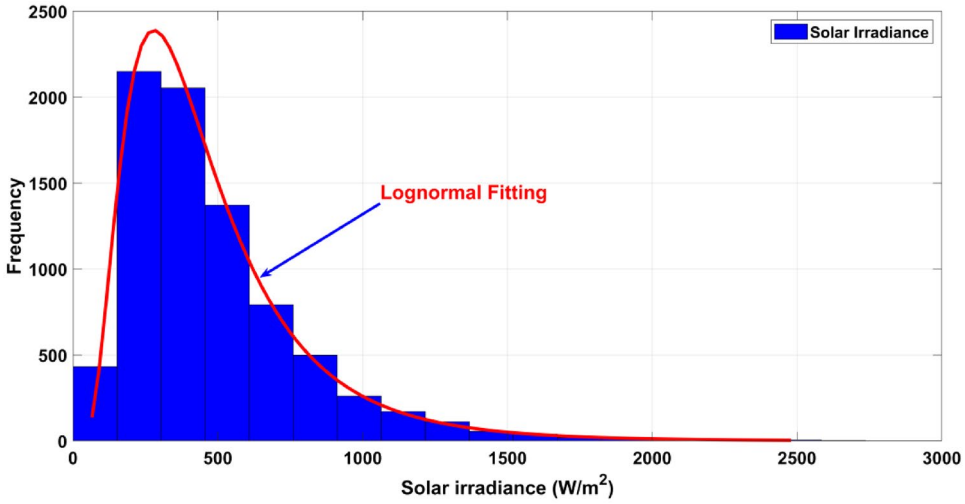

Figure 3. Solar irradiance distribution for solar PV.

primarily emit water vapor. However, during the reformation of natural gas or other fuels, they may produce some NO_X and CO_2 emissions[113,114]. Despite their higher initial costs, fuel cells are generally more efficient and have lower emissions compared to microturbines. In this paper, a typical low-voltage (LV) microgrid is considered, incorporating various DGs such as microturbines (MT), low-temperature fuel cells (PAFC), photovoltaic (PV) arrays, wind turbines (WT), and storage devices like lead-acid batteries[78]. It is assumed that all DG sources generate active power at unity power factor without requesting or producing reactive power. Additionally, a power exchange link exists between the microgrid and the utility (LV network), facilitating energy trading throughout various hours of the day based on decisions made by the microgrid central controller (MGCC).

Results and discussion

The microgrid test system under examination comprises a distributor and various distributed generators (DGs), including photovoltaic panels (PV), wind turbines (WT), microturbines (MT), fuel cells (FC), and batteries[92]. In the proposed model, the objective function aggregates the total cost of the microgrid, encompassing power generation costs and startup/shutdown costs of units, in addition to the net emission of pollutants. This problem is addressed through three distinct scenarios. The primary case, where all units are dispatched based on their actual constraints. In the second scenario, both the wind turbine (WT) and solar photovoltaic (PV) systems operate at their maximum output levels. In the third scenario, the utility is treated as an unbounded unit that can exchange energy with the microgrid without any constraints. The total load demand within the microgrid for a typical day includes primarily residential areas, one industrial feeder serving a small workshop, and one feeder with light commercial consumers, as documented in Ref.[92]. The cumulative energy demand for the specified day amounts to 1695 kilowatt-hours (kWh). Furthermore, the study takes into account the real-time variation in energy prices in the market for the specified day, as documented in the earlier study[92]. To ensure the flexible operation of the microgrid, the optimization algorithm dynamically assigns "on" or "off" states to three distributed generation (DG) units—MT (Micro Turbine), PV (Photovoltaic), and WT (Wind Turbine)—during the power dispatch problem, considering both objectives. Similarly, since the microgrid operates in grid-connected mode, the utility is consistently set to the "on" state. In order to comprehensively evaluate the impact of the battery and PAFC (Proton Exchange Membrane Fuel Cell) on grid operation and to maximize the benefits of these resources, the "on" state is deliberately chosen for these respective units. The minimum and maximum generation limits of the DG sources are obtained from Ref.[92]. Furthermore, the bid coefficients in cents of Euro (€ct) per kWh, as well as emissions in kilograms per MWh, assumed by the DG sources, are extracted from Ref.[92]. To streamline our analysis, all units under consideration in this research study are assumed to operate exclusively in electricity mode, without requiring heat during the analyzed period. It's important to highlight that the enhanced integration of renewable energies stands as a key motivation behind micro-grid installations. In actual micro-grid operations, forecasts of future requirements are crucial for preparing flexible systems to respond appropriately. Although renewable energy may not follow traditional operational patterns, its behavior can be anticipated, and forecast information becomes crucial for optimizing system efficiency within microgrids. In this study, the power output of photovoltaic (PV) and wind turbine (WT) units is projected using an expert prediction model. However, this aspect falls beyond the scope of the current paper and will be addressed in future research. Table 3 provides an overview of the forecasted output of these units. The maximum allowable daily power extracted from the PV and WT are taken from the earlier study[92]. The daily load power and the energy market price in the typical micro-grid considered are taken from Ref.[92].

To assess the effectiveness of the suggested SaCryStAl technique, a simulation is conducted comprising 50 trial runs aimed at minimizing operating costs. The controlling parameters of the proposed algorithm are selected as population size of 30 and maximum iteration of 1000[78]. The input data, including bids, technical coefficients, and emission coefficients of the DG sources for the microgrid test system under consideration, are sourced from

Hour	WT(kW)	PV(kW)	Load (kW)	Electrical energy price €ct/kWh
1	1.7850	0	52.00	0.2300
2	1.7850	0	50.00	0.1900
3	1.7850	0	50.00	0.1400
4	1.7850	0	51.00	0.1200
5	1.7850	0	56.00	0.1200
6	0.9150	0	63.00	0.2000
7	1.7850	0	70.00	0.2300
8	1.3050	0.200	75.00	0.3800
9	1.7850	3.750	76.00	2.5000
10	3.0900	7.525	80.00	4.0000
11	8.7750	10.45	78.00	4.0000
12	10.410	11.95	74.00	4.0000
13	3.9150	23.90	72.00	1.5000
14	2.3700	21.05	72.00	4.0000
15	1.7850	7.875	76.00	2.0000
16	1.3050	4.225	80.00	1.9500
17	1.7850	0.550	85.00	0.6000
18	1.7850	0	88.00	0.4100
19	1.3020	0	90.00	0.3500
20	1.7850	0	87.00	0.4300
21	1.3005	0	78.00	1.1700
22	1.3005	0	71.00	0.5400
23	0.9150	0	65.00	0.3000
24	0.6150	0	56.00	0.2600

Table 3. Predicted values of WT and PV[92].

Ref.[92]. Five distributed generation (DG) sources with associated characteristics generate electricity within the micro-grid. Any excess or shortfall of energy within the grid is balanced through exchange with the utility at the point of common coupling. All units, including the utility sourced from the macro grid, are obliged to operate within their power limits while meeting specified constraints. The output power levels of the wind turbine and solar cell based on the predicted values are presented in Table 3 [92].

Case-I: operation of distributed energy sources within prescribed bounds

The first test case analyzed in this study entails operating all distributed generators (DGs) and the grid within predefined constraints, as detailed in Table 4. Furthermore, Table 4 illustrates the optimal generation schedule for 24 h aimed at minimizing both cost and emissions. It is evident from Table 4 that, following the new approach, a substantial portion of the load is initially supplied by the fuel cell within the grid and utility via the point of common coupling during the early hours of the day. This preference is due to the lower bids of these units compared to others during this timeframe. As demand and utility bids rise in subsequent hours, distributed generation (DG) units adjust their output levels based on priority, prioritizing lower costs and emissions accordingly. Consequently, DG units start up sequentially as requested by the micro-grid regulatory controller and energy import from the macro grid is replaced by export actions to enhance revenue and reduce net emissions during this period. Additionally, it's worth noting that battery charging occurs during the early hours when prices are low, while discharge actions are postponed to midday when the load curve peaks. Furthermore, leveraging renewable energy sources such as wind and solar reduces pollution but may increase the operating cost. Hence, the utilization of energy from these resources should be constrained, taking into account emission and economic factors.

Tables 5 and 6 present the statistical outcomes of optimization algorithms, along with a concise comparison of their performances in the primary scenario. When evaluating performances based on both the best and worst solutions for cost and emission objectives, it becomes evident that the proposed optimization algorithm not only delivers superior outcomes but also demonstrates faster convergence. Additionally, statistical indices such as average and standard deviation further validate the algorithm's advantage in the optimization process. Tables 5 and 6 showcase standard deviation values for cost and emission objectives with the new algorithm limited to 0.006 and 0.005, respectively, indicating the excellent performance of the proposed model. By incorporating an oppositional population mechanism during the optimization process, the proposed algorithm explores further enhancements in both performance characteristics and optimal solutions. To provide a deeper insight into SaCryStAl's performance, the convergence characteristics of SaCryStAl and CryStAl algorithms for the best solution and each single objective are separately illustrated in Figs. 2 and 3. The operation cost was minimized by assigning the weighting factor w as unity. The proposed algorithm provides the least operation cost of 124.15 €ct compared with CryStAl, FSAPSO[91], GA[91], GWO[91], PSO[91], WOA[91], and KH[91]. The optimization findings indicate

Hour	P_d(kW)	P_{pv}(kW)	P_{wt}(kW)	P_{mt}(kW)	P_{FC}(kW)	P_{Batt}(kW)	P_{grid}(kW)
1	52	0	0	13.87	25.32	− 4.52	17.32
2	50	0	0	17.33	22.83	10.25	− 0.41
3	50	0	0	11.92	26.11	0.42	11.55
4	51	0	0	7.89	20.86	− 0.63	22.87
5	56	0	0	20.93	20.25	5.91	8.91
6	63	0	0	12.84	29.55	4.59	16.02
7	70	0	0	24.83	30	9.54	5.63
8	75	0	0	20.32	27.95	11.82	14.91
9	76	0	1.57	23.78	30	13.99	6.66
10	80	12.13	3.24	30	30	27.84	− 23.21
11	78	12.13	8.42	27.45	30	30	− 30
12	74	4.51	11.22	27.33	30	29.91	− 28.97
13	72	1.24	1.63	28.57	29.78	28.21	− 17.43
14	72	7.85	4.16	30	29.98	30	− 29.99
15	76	1.45	2.33	28.31	30	30	− 16.09
16	80	1.15	0.55	28.31	28.18	28.36	− 6.55
17	85	2.31	0	20.23	30	19.13	13.33
18	88	0	0	22.35	30	11.43	24.22
19	90	0	0	21.14	25.87	21.17	21.82
20	87	0	0	24.97	29.98	4.93	27.12
21	78	0	0	21.32	29.92	30	− 3.24
22	71	0	0	23.14	27.46	24.69	− 4.29
23	52	0	0	14.56	20.45	4.12	12.87
24	50	0	0	20.05	19.32	4.51	6.12

Table 4. Optimal generation schedule for minimization of operating cost and emission (Case-I).

Algorithm	Mean (€ct)	Standard deviation (€ct)	Max (€ct)	Min (€ct)	CPU time (s)
SaCryStAl	126.89	0.003	147.83	124.15	97.19
CryStAl	127.72	0.005	149.16	125.03	97.32
FSAPSO[91]	125.91	0.006	125.92	125.91	NA
GA[91]	151.89	36.23	210.46	125.91	114.67
GWO[91]	151.57	40.20	824.30	128.93	132.17
PSO[91]	145.28	53.52	830.83	126.16	556.64
WOA[91]	129.05	8.99	307.55	126.09	149.17
KH[91]	148.57	0.009	1337.7	105.94	104.17

Table 5. Statistical comparative results with other algorithms for minimization of operating cost (Case-I).

Algorithm	Mean (kg)	Standard deviation (kg)	Max (kg)	Min (kg)	CPU time (s)
SaCryStAl	420.96	0.002	428.04	419.14	76.41
CryStAl	422.03	0.004	429.25	420.89	76.83
FSAPSO[91]	422.02	0.005	422.03	422.02	NA
GA[91]	506.78	89.25	680.33	422.02	119.85
GWO[91]	580.88	300.97	2699.2	451.54	167.44
PSO[91]	500.44	216.42	2943.4	425.43	523.87
WOA[91]	428.79	68.54	2135.3	423.25	124.92
KH[91]	436.59	0.004	118.97	420.57	79.41

Table 6. Statistical comparison of results with other algorithms for emission minimization (Case-I).

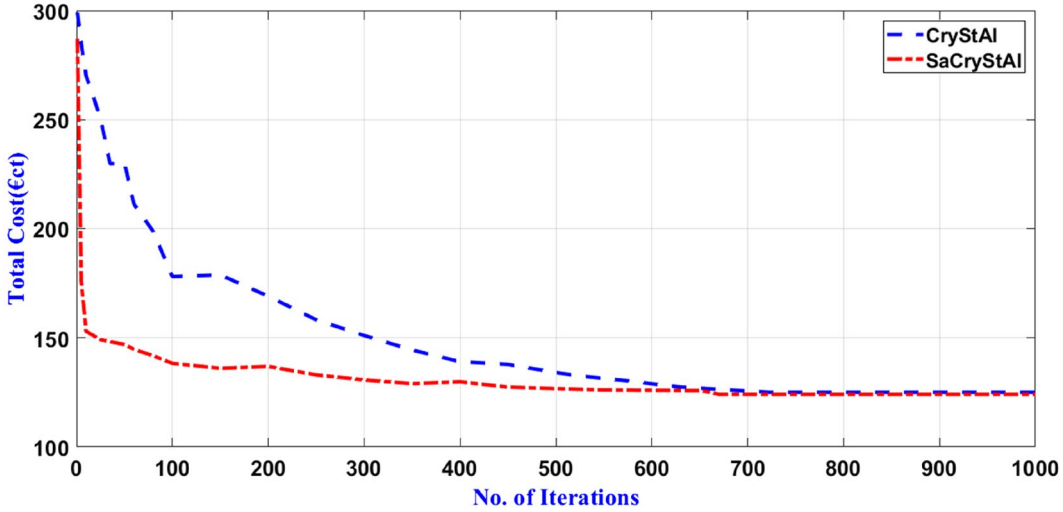

Figure 4. Convergence characteristic for the minimization of operating cost (Case-I).

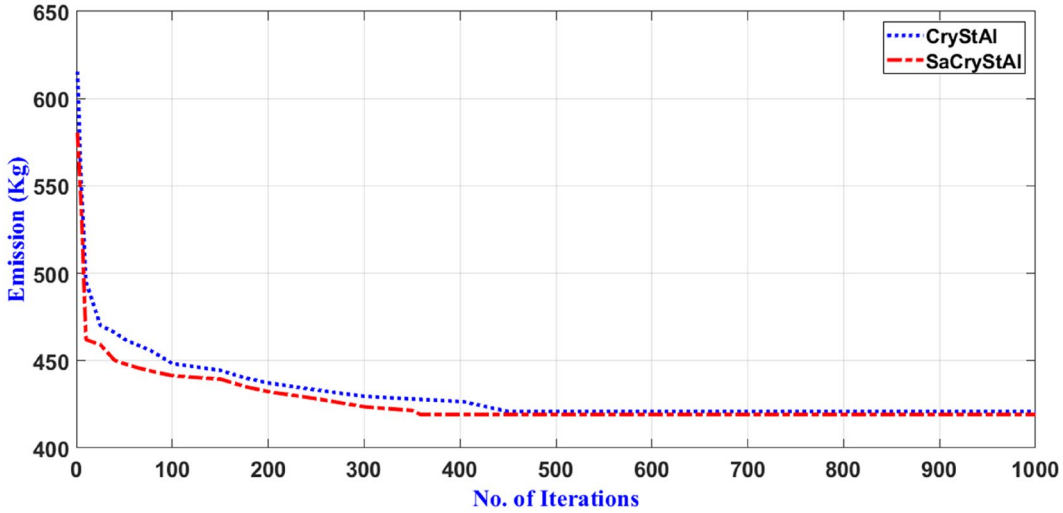

Figure 5. Convergence profile for emission minimization (Case-I).

a close alignment between the minimum operating cost and its mean value, underscoring the precision of the proposed algorithm. By adjusting the weighting factor from 1 to 0, we achieved an optimal emission value of 419.14 kg. Figures 4 and 5 depict that the cost objective function reaches its minimum after around 670 iterations with the new method and remains stable thereafter, contrasting with the CryStAl algorithm, which converges in approximately 690 iterations. Similarly, the emission objective function reaches its minimum after about 428 iterations with the new method, while the CryStAl algorithm converges in about 417 iterations. Additionally, Fig. 6 highlights the superior performance of all mentioned algorithms when considering both objectives. Employing a fuzzy logic approach enabled the proposed algorithm to achieve the global best compromise solution for both generations cost and emission minimization.

Figure 6 depicts the Pareto fronts of the respective trade-off objectives obtained from various comparison methods, alongside the best compromise solutions. Additionally, the distribution of non-dominated solutions along the Pareto optimal front, as observed in Fig. 6, validates the effectiveness of the proposed algorithm in addressing nonlinear multi-objective optimization problems. Moreover, the computational time for both operating cost and emission minimization using the proposed algorithm is notably shorter, indicating the high solution quality achieved. Overall, the optimization results strongly support the proposed algorithm's capability to address challenges related to equality and inequality in energy management problems.

Case-II: operation of microgrid with rated wind power

The WT is run at its rated power of 15 kW in the second scenario that is taken into consideration[115]. In this scenario, the proposed SaCryStAl is used to distribute the load to the MG components. While the PV generation is nil and the battery is in the charging stage, the MT, WT, FC, and grid actively contribute to meeting the

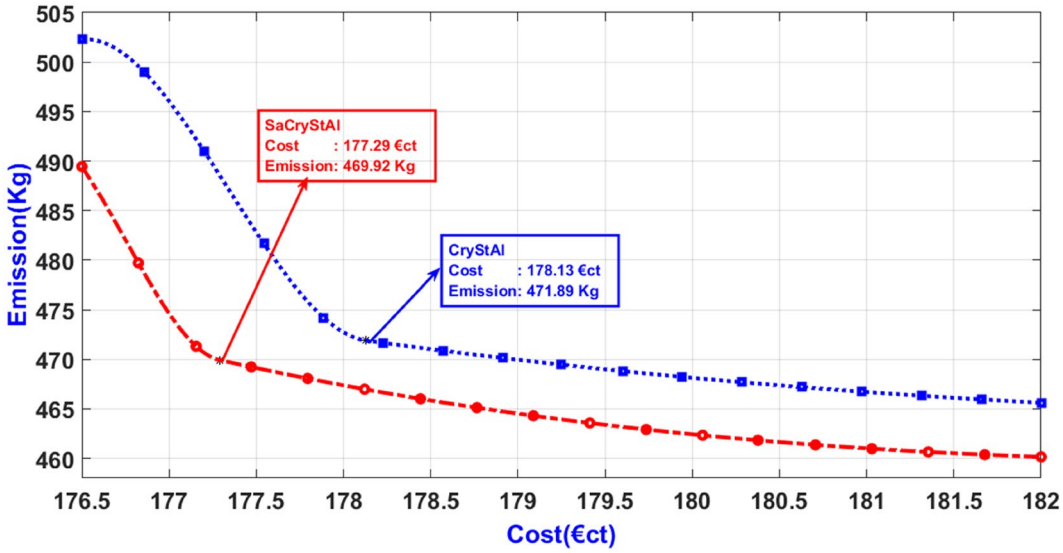

Figure 6. Trade-off characteristic between emissions and costs (Case-I).

Hour	P_d(kW)	P_{pv}(kW)	P_{wt}(kW)	P_{mt}(kW)	P_{FC}(kW)	P_{Batt}(kW)	P_{grid}(kW)
1	52	0	15	24.0394	7.4902	− 24.5295	30
2	50	0	15	12.9382	22.0562	− 29.9921	30
3	50	0	15	29.984	19.05328	− 30	15.9641
4	51	0	15	22.1806	14.9835	− 30	28.8297
5	56	0	15	29.9752	12.6371	− 30	28.3875
6	63	0	15	29.9806	29.9812	− 30	18.0382
7	70	0	15	29.9997	24.9988	− 30	30
8	75	0.263	15	29.9542	29.9732	− 30	29.813
9	76	3.26	15	27.5054	29.9239	30	− 29.6893
10	80	7.603	15	29.9231	4.7821	30	− 7.3029
11	78	11.289	15	29.8834	29.2381	16.8032	− 24.2131
12	74	14.093	15	12.0971	30	30	− 27.1892
13	72	24.752	15	29.9837	30	2.2645	− 30
14	72	23.198	15	10.2093	15.3921	18.9835	− 10.7824
15	76	8.0732	15	27.3891	22.0891	30	− 27.5498
16	80	6.309	15	29.6034	29.1138	29.7023	− 29.7213
17	85	1.752	15	29.5402	30	30	− 21.2874
18	88	0	15	29.7835	30	30	− 16.7832
19	90	0	15	22.6131	30	− 15	22.3891
20	87	0	15	28.0372	30	30	− 16.0348
21	78	0	15	29.6608	30	30	− 26.6608
22	71	0	15	30	30	25.9874	− 29.9874
23	65	0	15	30	20	− 29.9752	29.9752
24	56	0	15	30	12.9098	28.0733	− 29.9823

Table 7. Optimal generation schedule for minimization of operating cost and emission (Case-II).

electrical load during the first eight hours. The PV began to share the load with the other mounted devices during the second interval. In this instance, extra electricity is sold to the grid. The load is supported during the last hours by WT, MT, FC, and battery[115]. Table 7 lists the best outcomes and statistical variables that were taken into account in this situation. Setting the weighting factor to 1 prioritizes the minimization of operating costs. Figure 7 illustrates the convergence characteristics achieved by SaCryStAl and CryStAl for operating cost minimization. To minimize emissions, the weighting factor 'w' is set to 0, as shown in Fig. 8. SaCryStAl achieved the lowest operating cost of 53.92 €ct, while CryStAl yielded the maximum of 371.28 €ct. SaCryStAl also demonstrated

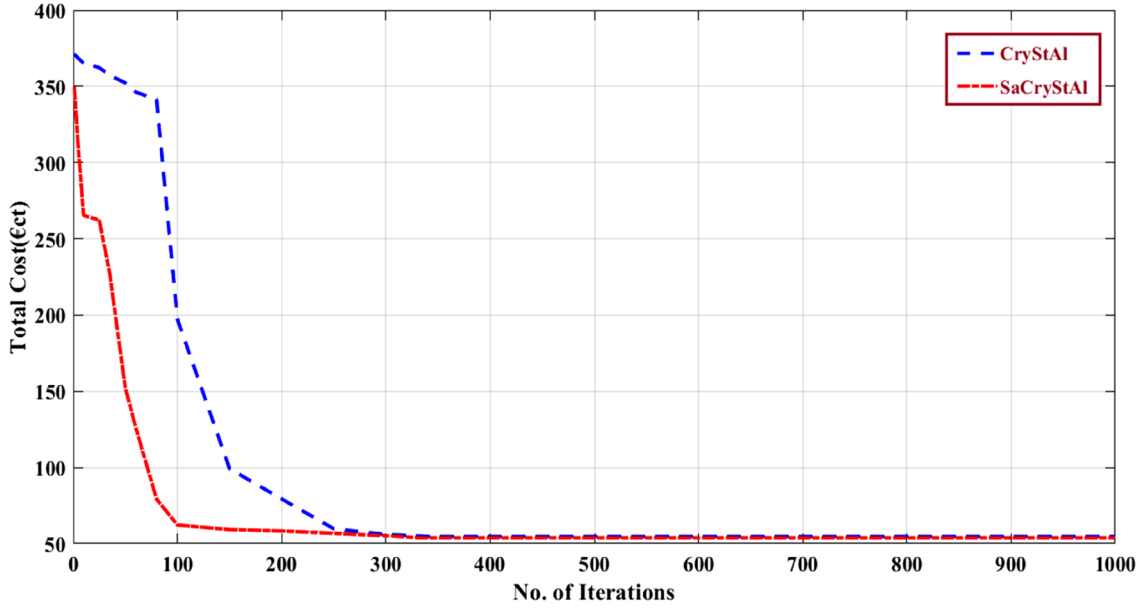

Figure 7. Convergence characteristic for the minimization of operating cost (Case-II).

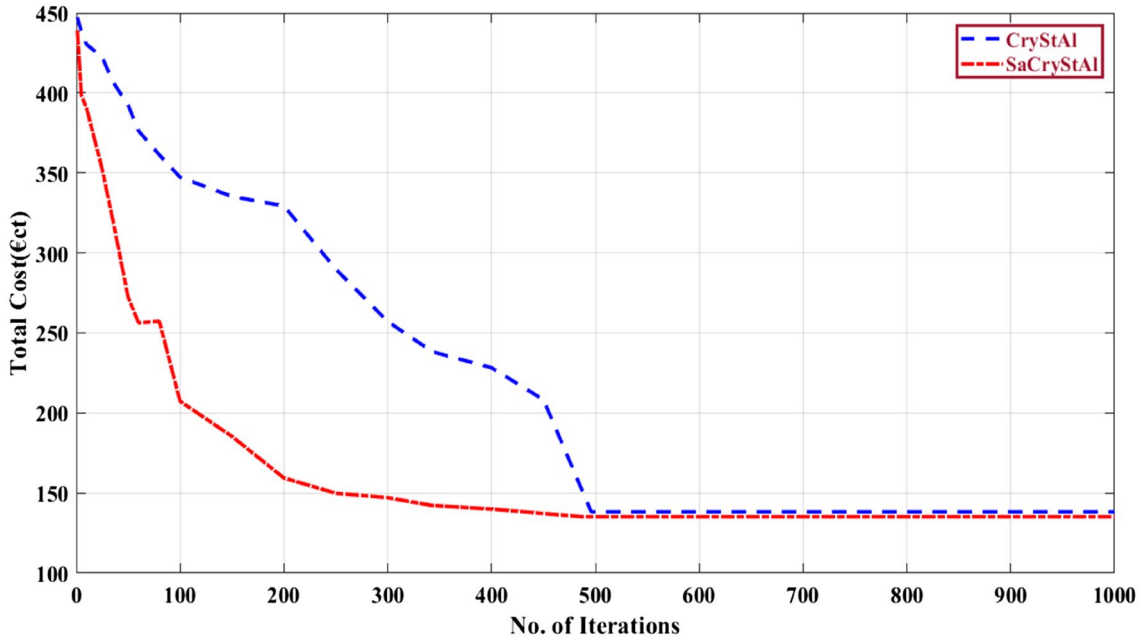

Figure 8. Convergence profile for emission minimization (Case-II).

superior variance, standard deviation, and elapsed time. In terms of emissions, SaCryStAl produced the least at 135.186 kg, whereas CryStAl reached a maximum of 439.0481 kg. Detailed results are summarized in Tables 8 and 9. Decreasing the weighting factor 'w' from 1 to 0 in steps of 0.001 generates compromise solutions where operating costs increase and emissions decrease simultaneously. Tables 8 and 9 provide a statistical comparison of optimization results for operating cost and emissions, respectively. Through a fuzzy logic approach, the proposed algorithm achieved the global best compromise solution for both objectives. Figure 9 illustrates the trade-off relationship between operating cost and emissions achieved through the utilization of SaCryStAl and CryStAl algorithms. Table 10 presents the comparison of best comparison solution obtained using SaCryStAl, CryStAl and other optimization algorithms for Case I and II. The proposed SaCryStAl algorithm provided a better optimal solution compared to CryStAl. This aims to excel, particularly with the distinctly differentiated Pareto front achieved by SaCryStAl for complex nonlinear optimization problems. In terms of fitness value variation, the SaCryStAl performed well in both goals since it quickly arrived at the best answer. Additionally, SaCryStAl exhibited shorter computational times compared to other optimization algorithms. The optimization results strongly support SaCryStAl's capability to address the complexities of both equality and inequality present in

Algorithm	Operating cost (€ct)						CPU time (s)
	Min	Max	Mean	Median	Variance	Std. dev	
SaCryStAl	53.92	349.74	56.79	109.25	17.8127	4.1805	551.684
CryStAl	54.75	371.28	57.46	112.37	18.1084	4.2358	573.841
HBA[115]	55.58	435.65	60.39	55.58	18.3	4.2779	614.053
DAOA[115]	56.676	535.89	134.53	139.22	18.681	4.3222	784.503
ARO[115]	55.724	630.61	67.508	56.44	18.417	4.2914	840.684
TDO[115]	55.582	939.29	63.146	56.291	18.301	4.278	1144.693
CHIO[115]	60.165	933.87	97.845	67.705	19.928	4.4641	1250.64
MRFO[115]	57.764	434.75	72.105	63.149	19.567	4.4234	1575.98
AO[115]	63.4926	722.509	278.832	337.697	22.131	4.7043	1584.589

Table 8. Statistical analysis of optimization results for operating cost minimization (Case-II).

Algorithm	Emission (kg)						CPU time (sec)
	Min	Max	Mean	Median	Variance	Std. dev	
SaCryStAl	135.186	439.048	138.905	154.49	0.5629	0.0237	597.062
CryStAl	138.205	447.204	140.752	157.282	0.5803	0.0243	599.604
HBA[115]	137.008	708.795	141.685	137.65	0.0006	0.0246	607.052
DAOA[115]	324.958	459.245	356.798	358.102	12.1629	3.4875	651.459
ARO[115]	145.945	600.313	157.656	146.073	0.6042	0.7773	790.374
TDO[115]	145.944	752.899	148.77	145.946	0.6042	0.7773	1069.83
AO[115]	146.876	744.895	207.053	207.112	0.5858	0.7654	1142.79
MRFO[115]	146.171	550.711	158.956	147.267	0.5985	0.7736	1176.13
CHIO[115]	159.634	658.708	211.261	187.347	0.9825	0.9912	1507.5

Table 9. Statistical analysis of optimization results for emission minimization (Case-II).

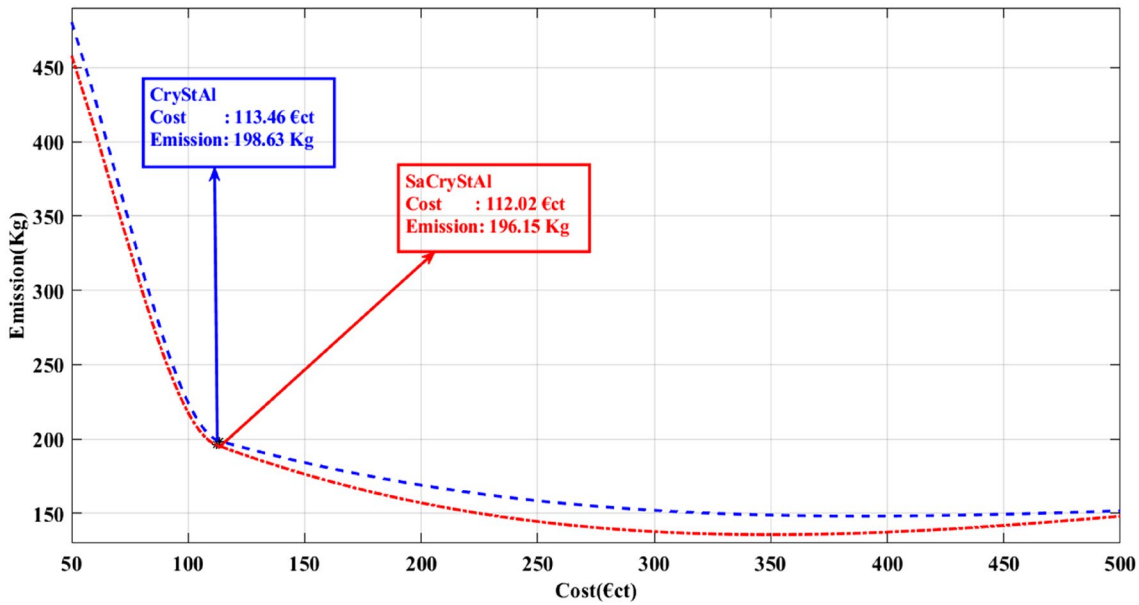

Figure 9. Trade-off characteristic between emissions and costs (Case-II).

microgrid energy management challenges, particularly with the incorporation of RES and PHEVs. The obtained simulation results showed excellent performance when WT was operating at its rated power.

Algorithm		SaCryStAl	CryStAl	ALO[91]	FSAPSO[91]	Lexicographic optimization algorithm[110]
Case-I	Operating cost (€ct)	177.29	178.13	187.81	191.042	180.4
	Emission (kg)	469.92	471.89	473.12	721.076	529.3
Case-II	Operating cost (€ct)	112.02	113.46	NA	NA	NA
	Emission (kg)	196.15	198.63	NA	NA	NA

Table 10. Comparison of best compromise solution for Case-I and Case-II. *NA* not available.

Case-III: operation of microgrid integrated with PHEVs

In this analysis, the integration of PHEVs with the microgrid is explored. It is assumed that 30% of the 70 EVs are linked to the MG[77]. The objective in this scenario is to minimize operating costs. Here, the uncoordinated, coordinated, and intelligent charging modes of PHEVs are investigated. The optimal generation schedule of microgrid with the integration of PHEVs for the minimization of operating cost for uncoordinated, coordinated and smart charging modes are presented in Tables 11, 12 and 13 respectively. Table 14 presents the optimal value of the operation cost obtained using SaCryStAl and other optimization algorithms for the three different charging methods considered. It is evident from the optimization results, the proposed SaCryStAl performed better than CryStAl algorithm. In the uncoordinated, coordinated, and smart charging modes, the SaCryStAl algorithm attained optimal fitness values of 319.9301 €ct, 160.9827 €ct, and 128.2815 €ct, respectively. Figures 10, 11 and 12 present the convergence characteristics for the minimization of operating cost for uncoordinated, coordinated and smart charging modes respectively. The convergence behavior curve regarding operating cost minimization demonstrates that the proposed SaCryStAl algorithm exhibits smoother and more rapid convergence compared to the CryStAl algorithm across all three charging modes investigated. Moreover, Figs. 10, 11, and 12 illustrate that the SaCryStAl algorithm delivers swift and resilient performance, effectively mitigating optimization challenges encountered in diverse power systems. In order to supply the PHEVs from the MG, there is a limitation in the utility generating to acquire the full power capabilities. When using coordinated and smart charging modes, there is less integration between MT and the grid. As a result, both modes' running costs are better than the uncoordinated charging mode's. According to Tables 11, 12 and 13, the FC serves as the primary energy source during the day, with the grid being used at night and in the morning. MT generation is roughly constrained. The RESs and batteries assist in meeting the demand at midday, and any extra electricity is then sold to the grid.

Hour	P_d(kW)	P_{pv}(kW)	P_{wt}(kW)	P_{mt}(kW)	P_{FC}(kW)	P_{Batt}(kW)	P_{grid}(kW)
1	52	0	2.39	29.99	22.5	− 30	59.99
2	50	0	2.42	29.99	5	− 18.91	60
3	50	0	2.51	29.75	21.52	− 27.75	57.25
4	51	0	2.48	29.62	28.3	− 27.75	50.16
5	56	0	2.44	29.64	21.88	− 20	54.75
6	63	0	1.22	29.99	30.99	− 31.99	59.99
7	70	0	2.43	29.99	31.65	− 19.72	59.99
8	75	0	2.37	29.99	30.55	− 32.97	59.99
9	76	4.29	4.99	29.91	34.99	58.91	− 11.92
10	80	7.51	10.55	29.82	37.75	59.34	− 19.93
11	78	10.31	19.25	29.82	36.51	59.34	− 19.99
12	74	19.25	22.55	29.74	46.73	44.21	− 23.29
13	72	22.65	27.72	29.74	34.2	47.23	− 17.56
14	72	21.99	22.61	28.63	35.25	47.23	− 21.78
15	76	13.25	10.12	28.59	37.61	59.91	− 19.97
16	80	4.99	7.43	28.67	36.25	59.32	− 18.02
17	85	1.43	2.55	29.89	32.55	60	− 7.99
18	88	0	2.43	29.75	32.46	60	90.02
19	90	0	2.35	29.99	32.41	60	90.02
20	87	0	2.53	29.99	32.52	60	90.02
21	78	0	2.31	29.99	32.48	60	81.75
22	71	0	2.36	29.99	32.53	60	77.62
23	52	0	2.12	29.99	32.47	33.28	70.19
24	50	0	1.55	29.99	32.63	0	59.99

Table 11. Optimal generation schedule for minimization of operating cost for Case-III (uncoordinated charging).

Hour	P_d(kW)	P_{pv}(kW)	P_{wt}(kW)	P_{mt}(kW)	P_{FC}(kW)	P_{Batt}(kW)	P_{grid}(kW)
1	52	0	2.41	29.98	22.4	− 29.99	60
2	50	0	2.41	29.98	21.78	− 29.99	59.02
3	50	0	2.41	29.79	22.75	− 27.86	57.29
4	51	0	2.41	29.65	28.75	− 22.79	50.11
5	56	0	2.41	29.67	9.88	− 9.16	57.18
6	63	0	1.24	29.98	31.11	− 29.97	60
7	70	0	2.43	29.98	32.08	− 21.09	60
8	75	0	2.38	29.98	30.78	− 17.93	60
9	76	4.29	5.11	29.89	37.41	58.94	− 18.92
10	80	7.51	10.57	29.81	38.72	57.98	− 18.92
11	78	10.31	19.33	29.79	41.12	51.92	− 20
12	74	19.25	22.47	26.72	56.72	56.94	− 25.29
13	72	22.65	27.72	24.74	32.11	40.03	− 22.98
14	72	21.99	22.63	18.23	39.27	57.93	− 17.99
15	76	13.25	10.14	23.39	36.78	59.96	− 24.39
16	80	4.99	7.39	28.67	35.75	59.48	− 17.79
17	85	1.43	2.53	29.89	32.49	59.99	− 4.99
18	88	0	2.41	29.75	31.24	59.99	− 3.28
19	90	0	2.34	29.94	30.89	2.13	60
20	87	0	2.57	29.94	30.02	59.99	− 4.82
21	78	0	2.32	29.94	30.91	59.99	80.93
22	71	0	2.34	29.94	30.34	59.99	77.18
23	52	0	2.13	29.94	30.31	25.78	70.21
24	50	0	1.53	29.98	30.12	0	60

Table 12. Optimal generation schedule for minimization of operating cost for Case-III (coordinated charging).

Hour	P_d(kW)	P_{pv}(kW)	P_{wt}(kW)	P_{mt}(kW)	P_{FC}(kW)	P_{Batt}(kW)	P_{grid}(kW)
1	52	0	2.44	30	22.78	− 30	60
2	50	0	2.44	30	20	− 30	60
3	50	0	2.44	28.39	5.12	− 7.98	58.13
4	51	0	2.44	30	32.12	− 5.48	60
5	56	0	1.29	30	32.12	− 1.28	60
6	63	0	2.43	30	31.78	− 29.99	60
7	70	0	2.09	30	31.29	− 21.18	60
8	75	0	2.43	30	33.13	− 17.89	60
9	76	5.15	2.39	29.12	32.78	59.02	− 19.18
10	80	7.63	6.99	28.29	37.01	56.29	− 17.28
11	78	10.09	18.98	23.91	45.12	51.18	− 21.89
12	74	12.89	21.99	18.12	49.14	47.12	− 24.71
13	72	24.92	28.19	27.97	51.29	49.12	− 27.89
14	72	20.18	22.87	30	44.89	49.89	− 30
15	76	9.12	10.09	28.92	38.19	57.92	− 19.94
16	80	5.23	7.59	30	32.01	59.78	− 9.83
17	85	1.46	2.71	30	31.29	60	− 3.75
18	88	0	2.48	30	30.98	60	− 2.16
19	90	0	2.33	30	31.89	− 1.89	60
20	87	0	2.48	30	32.98	60	− 2.56
21	78	0	2.43	30	31.87	60	− 9.99
22	71	0	2.43	30	31.87	60	− 20
23	52	0	2.09	30	30.99	− 27.13	60
24	50	0	1.49	30	27.99	− 30	60

Table 13. Optimal generation schedule for minimization of operating cost for Case-III (smart charging).

Algorithm	Uncoordinated charging (€ct)	Coordinated charging (€ct)	Smart charging (€ct)
SaCryStAl	319.9301	160.9827	128.2815
CryStAl	320.8627	161.9064	129.0953
GSA-PS[78]	675.4259	390.4521	337.2845
BES[78]	321.7595	162.7251	129.8758
RUN[78]	322.0152	164.2675	131.5451
MGO[78]	322.2636	162.7319	132.6798
CBOA[78]	407.3604	242.3315	197.7891
BWO[78]	327.7516	175.3402	148.7032
DO[78]	328.1547	178.6087	142.4507

Table 14. Analysis of simulation results for minimizing operating costs across three charging modes.

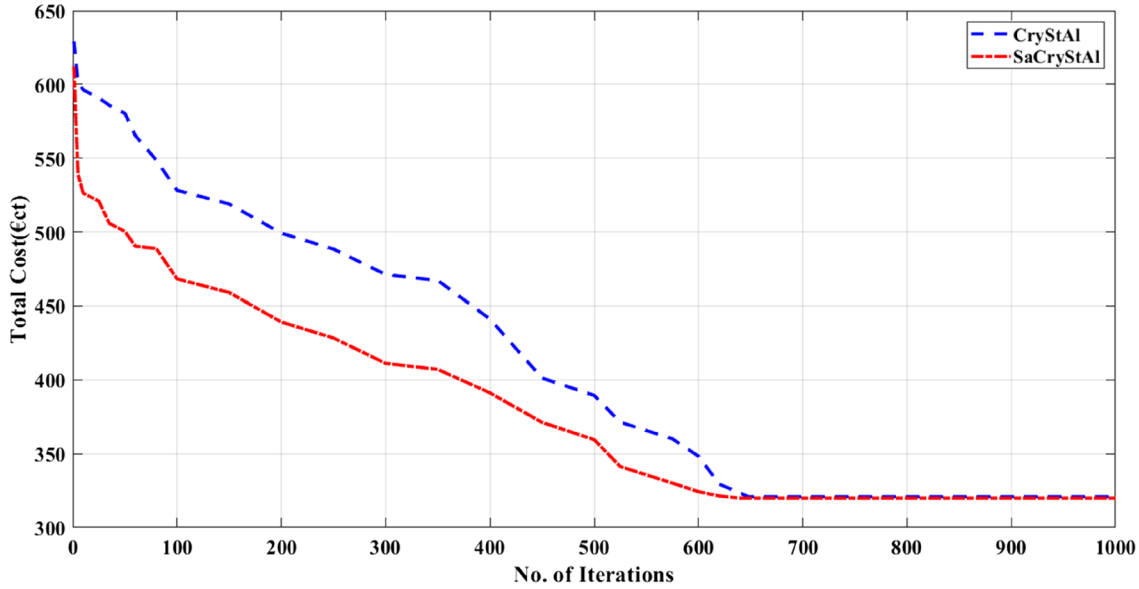

Figure 10. Convergence characteristic for the minimization of operating cost (uncoordinated charging mode).

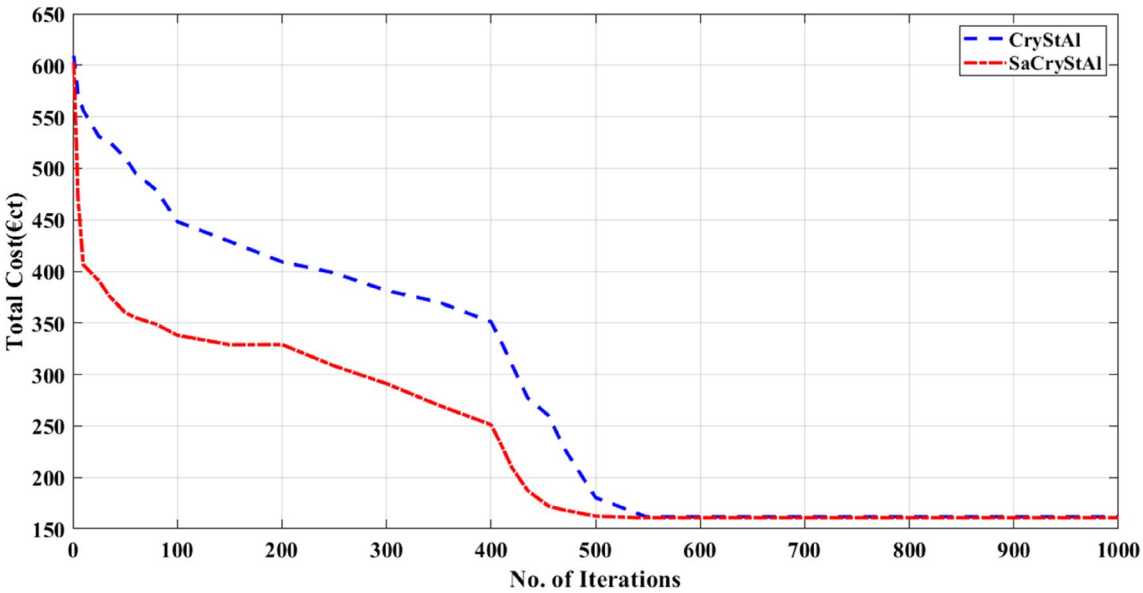

Figure 11. Convergence characteristic for the minimization of operating cost (coordinated charging mode).

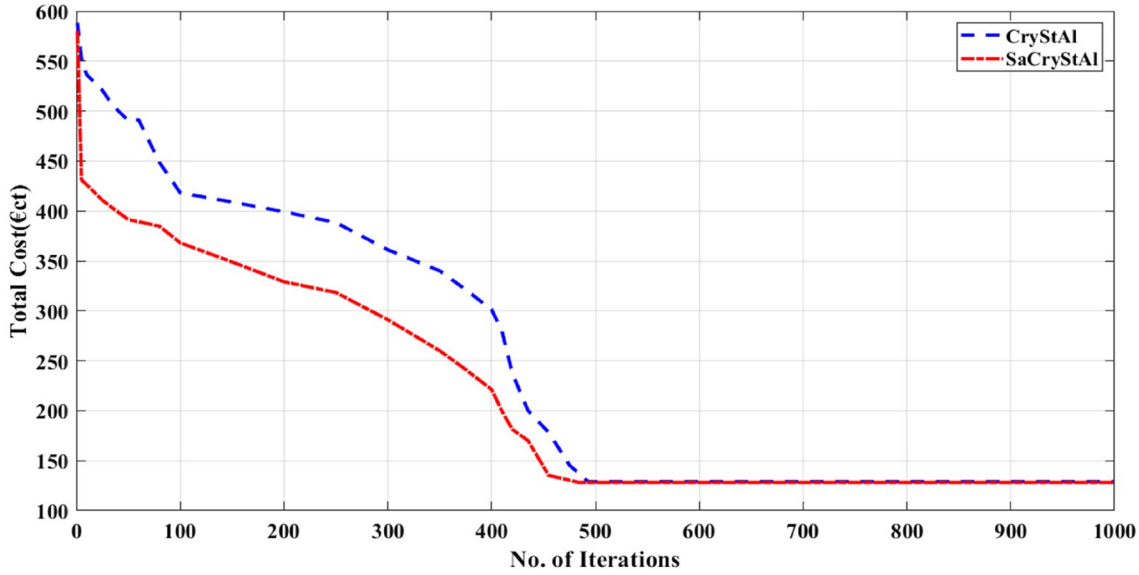

Figure 12. Convergence characteristic for the minimization of operating cost (smart charging mode).

In this case, the recommended energy management technique outperformed the other optimizers taken into consideration to produce the best operating costs for MG with PHEVs.

Conclusion and future research directions

This research implemented a new energy management technique for MGs with installed RESs and PHEVs that incorporates the SaCryStAl algorithm. The suggested method is accountable for distributing energy among many units. In the grid-connected MG, fuel cells, storage batteries, plug-in hybrid electric vehicles (PHEVs), nonrenewable sources (MT), and renewable generators (PV and WT) are all taken into consideration. The objectives taken into account in this effort include lowering the MG operating cost and reducing pollutant emission. In order to compare the performance of the proposed algorithm to currently used evolutionary optimization approaches, the study took into account three different scenarios. The research investigated three different scenarios to assess the effectiveness of the proposed algorithm compared to conventional CryStAl and other optimization techniques. The authors conducted simulations for each scenario and compared the results. In the first scenario, the SaCryStAl algorithm, designed for single-objective optimization, successfully achieved optimal solutions for cost and emissions, recording 124.15 €ct and 419.14 kg, respectively, within acceptable time frames of 97.19 and 76.41 s respectively. Optimization result surpassed those of other existing optimization algorithms. In the second scenario, the SaCryStAl algorithm once again provided superior results, delivering optimal cost and emission values of 53.92 €ct and 135.186 kg, respectively, within acceptable computational times of 551.684 and 597.062 s respectively. In the third scenario, the SaCryStAl algorithm maintained its success by achieving optimal operation costs of 319.9301 €ct, 160.9827 €ct, and 128.2815 €ct for the uncoordinated, coordinated, and smart charging modes of PHEVs, respectively. Moreover, the SaCryStAl algorithm demonstrated strong performance in optimizing both cost and emissions within a multi-objective framework. In the first scenario, it achieved optimal operational cost and emissions of 177.29 €ct and 469.92 kg respectively. In the second scenario, the algorithm produced even better results with optimal operational cost and emissions of 112.02 €ct and 196.15 kg respectively. The study's findings suggest that widespread use of PHEVs and RES will have a significant impact on grid functioning in terms of emission goals. The SaCryStAl algorithm demonstrates remarkable stability, convergence, and performance, as evidenced by the numerical results. Notably, it yields a diverse collection of Pareto-optimal solutions that are evenly distributed. This abundance of options empowers system operators to select the most suitable power dispatch strategy to meet their economic and environmental objectives effectively. Furthermore, our proposed method outperforms other optimization algorithms in terms of both economic and environmental outcomes. Remarkably, despite its superior performance, the computational time of our approach remains practically identical to that of the conventional CryStAl. Moreover, our current research extends beyond mere optimization by incorporating market pricing, load, photovoltaic (PV), and wind turbine (WT) uncertainties. This holistic approach ensures the optimal scheduling of microgrid operations, considering real-world uncertainties and enhancing the robustness of our findings.

In the future, a stochastic model that takes into account hydrothermal units as well as renewable energy sources could be offered. The proposed model's influence on pollutant emissions can be thoroughly examined, and market prices and tariff structures can also be taken into account. In considering future research directions, several promising avenues emerge from this study's findings. Firstly, further investigation into the integration of emerging technologies, such as advanced energy storage systems and demand response mechanisms, could enhance the efficiency and resilience of microgrid operations. Additionally, exploring the applicability of the proposed SaCryStAl algorithm in larger-scale energy systems and diverse geographical contexts would be beneficial. Furthermore, incorporating real-time data analytics and machine learning techniques could augment the

algorithm's decision-making capabilities, enabling more adaptive and proactive energy management strategies. Lastly, exploring the socio-economic implications of microgrid integration and assessing the potential barriers to adoption could provide valuable insights for policymakers and industry stakeholders. By addressing these research avenues, future studies can contribute to advancing the state-of-the-art in microgrid optimization and facilitating the transition towards sustainable and resilient energy systems.

Data availability

The datasets used and/or analysed during the current study available from the corresponding author on reasonable request.

Received: 8 February 2024; Accepted: 3 July 2024
Published online: 08 July 2024

References

1. Rekioua, D. *et al.* Optimization and intelligent power management control for an autonomous hybrid wind turbine photovoltaic diesel generator with batteries. *Sci. Rep.* **13**, 21830. https://doi.org/10.1038/s41598-023-49067-4 (2023).
2. Yang, C. *et al.* Optimized integration of solar energy and liquefied natural gas regasification for sustainable urban development: Dynamic modeling, data-driven optimization, and case study. *J. Clean. Prod.* **447**, 141405. https://doi.org/10.1016/j.jclepro.2024.141405 (2024).
3. Zhou, X., Cai, Y. & Li, X. Process arrangement and multi-aspect study of a novel environmentally-friendly multigeneration plant relying on a geothermal-based plant combined with the goswami cycle booted by kalina and desalination cycles. *Energy* **299**, 131381. https://doi.org/10.1016/j.energy.2024.131381 (2024).
4. Ravindran, M. A. *et al.* A novel technological review on fast charging infrastructure for electrical vehicles: Challenges, solutions, and future research directions. *Alex. Eng. J.* **82**, 260–290. https://doi.org/10.1016/j.aej.2023.10.009 (2023).
5. Cao, B. *et al.* Hybrid microgrid many-objective sizing optimization with fuzzy decision. *IEEE Trans. Fuzzy Syst.* **28**, 2702–2710. https://doi.org/10.1109/TFUZZ.2020.3026140 (2020).
6. Panda, S. *et al.* A comprehensive review on demand side management and market design for renewable energy support and integration. *Energy Rep.* **10**, 2228–2250. https://doi.org/10.1016/j.egyr.2023.09.049 (2023).
7. Li, P., Hu, J., Qiu, L., Zhao, Y. & Ghosh, B. K. A distributed economic dispatch strategy for power-water networks. *IEEE Trans. Control Netw. Syst.* **9**, 356–366. https://doi.org/10.1109/TCNS.2021.3104103 (2022).
8. Duan, Y., Zhao, Y. & Hu, J. An initialization-free distributed algorithm for dynamic economic dispatch problems in microgrid: Modeling, optimization and analysis. *Sustain. Energy, Grids Netw.* **34**, 101004. https://doi.org/10.1016/j.segan.2023.101004 (2023).
9. Kumar, B. A. *et al.* A novel framework for enhancing the power quality of electrical vehicle battery charging based on a modified Ferdowsi converter. *Energy Rep.* **10**, 2394–2416. https://doi.org/10.1016/j.egyr.2023.09.070 (2023).
10. Shirkhani, M. *et al.* A review on microgrid decentralized energy/voltage control structures and methods. *Energy Rep.* **10**, 368–380. https://doi.org/10.1016/j.egyr.2023.06.022 (2023).
11. Sahoo, G. K., Choudhury, S., Rathore, R. S., Bajaj, M. & Dutta, A. K. Scaled conjugate-artificial neural network-based novel framework for enhancing the power quality of grid-tied microgrid systems. *Alex. Eng. J.* **80**, 520–541. https://doi.org/10.1016/j.aej.2023.08.081 (2023).
12. Wang, C., Wang, Y., Wang, K., Dong, Y. & Yang, Y. An improved hybrid algorithm based on biogeography/complex and metropolis for many-objective optimization. *Math. Probl. Eng.* **2017**, 1–14. https://doi.org/10.1155/2017/2462891 (2017).
13. Sahoo, G. K., Choudhury, S., Rathore, R. S. & Bajaj, M. A novel prairie dog-based meta-heuristic optimization algorithm for improved control, better transient response, and power quality enhancement of hybrid microgrids. *Sensors* **23**, 5973. https://doi.org/10.3390/s23135973 (2023).
14. Lei, Y., Yanrong, C., Hai, T., Ren, G. & Wenhuan, W. DGNet: An adaptive lightweight defect detection model for new energy vehicle battery current collector. *IEEE Sens. J.* **23**, 29815–29830. https://doi.org/10.1109/JSEN.2023.3324441 (2023).
15. Azaroual, M. *et al.* Optimal solution of peer-to-peer and peer-to-grid trading strategy sharing between prosumers with grid-connected photovoltaic/wind turbine/battery storage systems. *Int. J. Energy Res.* **2023**, 1–17. https://doi.org/10.1155/2023/6747936 (2023).
16. Hou, M., Zhao, Y. & Ge, X. Optimal scheduling of the plug-in electric vehicles aggregator energy and regulation services based on grid to vehicle. *Int. Trans. Electr. Energy Syst.* **27**, e2364. https://doi.org/10.1002/etep.2364 (2017).
17. Choudhury, S. *et al.* Energy management and power quality improvement of microgrid system through modified water wave optimization. *Energy Rep.* **9**, 6020–6041. https://doi.org/10.1016/j.egyr.2023.05.068 (2023).
18. Iqbal, S. *et al.* Electric vehicles aggregation for frequency control of microgrid under various operation conditions using an optimal coordinated strategy. *Sustainability* **14**, 3108. https://doi.org/10.3390/su14053108 (2022).
19. Khosravi, N. *et al.* A novel control approach to improve the stability of hybrid AC/DC microgrids. *Appl. Energy* **344**, 121261. https://doi.org/10.1016/j.apenergy.2023.121261 (2023).
20. Karthik, N., Parvathy, A. K., Rajagopalan, A. & Baskar, S. A review of optimization techniques applied to solve unit commitment problem in microgrid. *Indones. J. Electr. Eng. Comput. Sci.* **15**, 1161. https://doi.org/10.11591/ijeecs.v15.i3.pp1161-1169 (2019).
21. Khan, N. H. *et al.* A novel modified artificial rabbit optimization for stochastic energy management of a grid-connected microgrid: A case study in China. *Energy Rep.* **11**, 5436–5455 (2024).
22. Nagarajan, K., Rajagopalan, A., Angalaeswari, S., Natrayan, L. & Mammo, W. D. Combined economic emission dispatch of microgrid with the incorporation of renewable energy sources using improved mayfly optimization algorithm. *Comput. Intell. Neurosci.* **2022**, 1–22. https://doi.org/10.1155/2022/6461690 (2022).
23. Sahri, Y. *et al.* Performance improvement of hybrid system based DFIG-Wind/PV/Batteries connected to DC and AC grid by applying intelligent control. *Energy Rep.* **9**, 2027–2043. https://doi.org/10.1016/j.egyr.2023.01.021 (2023).
24. Dhivya, S., Arul, R., Maheswari, S., Kanimozhi, R., Karthik, N. Optimal scheduling and sizing of energy storage system using hybrid algorithm for electric vehicles. In *2022 International Virtual Conference on Power Engineering Computing and Control: Developments in Electric Vehicles and Energy Sector for Sustainable Future (PECCON)*, 2022: pp. 1–5. https://doi.org/10.1109/PECCON55017.2022.9851152
25. Abraham, D. S. *et al.* Fuzzy-based efficient control of DC microgrid configuration for PV-energized EV charging station. *Energies* **16**, 2753. https://doi.org/10.3390/en16062753 (2023).
26. Pachauri, N. *et al.* A robust fractional-order control scheme for PV-penetrated grid-connected microgrid. *Mathematics* **11**, 1283. https://doi.org/10.3390/math11061283 (2023).
27. Chatterjee, S. *et al.* Optimal real-time tuning of autonomous distributed power systems using modern techniques. *Front. Energy Res.* **11**, 1055845. https://doi.org/10.3389/fenrg.2023.1055845 (2023).

28. Mohanty, S. *et al.* Demand side management of electric vehicles in smart grids: A survey on strategies, challenges, modeling, and optimization. *Energy Rep.* **8**, 12466–12490. https://doi.org/10.1016/j.egyr.2022.09.023 (2022).
29. Zandrazavi, S. F., Guzman, C. P., Pozos, A. T., Quiros-Tortos, J. & Franco, J. F. Stochastic multi-objective optimal energy management of grid-connected unbalanced microgrids with renewable energy generation and plug-in electric vehicles. *Energy* **241**, 122884. https://doi.org/10.1016/j.energy.2021.122884 (2022).
30. Panda, S. *et al.* Residential demand side management model, optimization and future perspective: A review. *Energy Rep.* **8**, 3727–3766. https://doi.org/10.1016/j.egyr.2022.02.300 (2022).
31. Sharma, S. *et al.* Modeling and sensitivity analysis of grid-connected hybrid green microgrid system. *Ain Shams Eng. J.* **13**, 101679. https://doi.org/10.1016/j.asej.2021.101679 (2022).
32. Abdalla, A. N. *et al.* Optimized economic operation of microgrid: Combined cooling and heating power and hybrid energy storage systems. *J. Energy Resour. Technol.* **143**, 070906. https://doi.org/10.1115/1.4050971 (2021).
33. Dashtdar, M., Bajaj, M. & Hosseinimoghadam, S. M. S. Design of optimal energy management system in a residential microgrid based on smart control. *Smart Sci.* **10**, 25–39. https://doi.org/10.1080/23080477.2021.1949882 (2022).
34. Dashtdar, M., Nazir, M. S., Hosseinimoghadam, S. M. S., Bajaj, M. & Goud, B. S. Improving the sharing of active and reactive power of the islanded microgrid based on load voltage control. *Smart Sci.* **10**, 142–157. https://doi.org/10.1080/23080477.2021.2012010 (2022).
35. Amoussou, I., Tanyi, E., Agajie, T., Khan, B. & Bajaj, M. Optimal sizing and location of grid-interfaced PV, PHES, and ultra capacitor systems to replace LFO and HFO based power generations. *Sci. Rep.* **14**, 8591. https://doi.org/10.1038/s41598-024-57231-7 (2024).
36. Mohapatra, B. *et al.* Optimizing grid-connected PV systems with novel super-twisting sliding mode controllers for real-time power management. *Sci. Rep.* **14**, 4646. https://doi.org/10.1038/s41598-024-55380-3 (2024).
37. Kumar, B. A. *et al.* Hybrid genetic algorithm-simulated annealing based electric vehicle charging station placement for optimizing distribution network resilience. *Sci. Rep.* **14**, 7637. https://doi.org/10.1038/s41598-024-58024-8 (2024).
38. Deghfel, N., Badoud, A. E., Merahi, F., Bajaj, M. & Zaitsev, I. A new intelligently optimized model reference adaptive controller using GA and WOA-based MPPT techniques for photovoltaic systems. *Sci. Rep.* **14**, 6827. https://doi.org/10.1038/s41598-024-57610-0 (2024).
39. Hou, H. *et al.* Multi-objective economic dispatch of a microgrid considering electric vehicle and transferable load. *Appl. Energy* **262**, 114489. https://doi.org/10.1016/j.apenergy.2020.114489 (2020).
40. Hu, J., Zou, Y. & Soltanov, N. A multilevel optimization approach for daily scheduling of combined heat and power units with integrated electrical and thermal storage. *Expert Syst. Appl.* **250**, 123729. https://doi.org/10.1016/j.eswa.2024.123729 (2024).
41. Huang, Z. *et al.* Economic-environmental scheduling of microgrid considering V2G-enabled electric vehicles integration. *Sustain. Energy, Grids Netw.* **32**, 100872. https://doi.org/10.1016/j.segan.2022.100872 (2022).
42. Jiao, F., Zou, Y., Zhang, X. & Zou, R. Multi-objective optimal energy management of microgrids including plug-in electric vehicles with the vehicle to grid capability for energy resources scheduling. *Proc. Inst. Mech. Eng. Part A J. Power Energy* **235**, 563–580. https://doi.org/10.1177/0957650920942998 (2021).
43. Mei, Y., Li, B., Wang, H., Wang, X. & Negnevitsky, M. Multi-objective optimal scheduling of microgrid with electric vehicles. *Energy Rep.* **8**, 4512–4524. https://doi.org/10.1016/j.egyr.2022.03.131 (2022).
44. Beyazıt, M. A., Taşcıkaraoğlu, A. & Catalão, J. P. S. Cost optimization of a microgrid considering vehicle-to-grid technology and demand response. *Sustain. Energy, Grids Netw.* **32**, 100924. https://doi.org/10.1016/j.segan.2022.100924 (2022).
45. Dharavat, N. *et al.* Optimal allocation of renewable distributed generators and electric vehicles in a distribution system using the political optimization algorithm. *Energies* **15**, 6698. https://doi.org/10.3390/en15186698 (2022).
46. Hai, T., Zhou, J., Alazzawi, A. K. & Muranaka, T. Management of renewable-based multi-energy microgrids with energy storage and integrated electric vehicles considering uncertainties. *J. Energy Storage* **60**, 106582. https://doi.org/10.1016/j.est.2022.106582 (2023).
47. Hai, T., Zhou, J. & Muranaka, K. Energy management and operational planning of renewable energy resources-based microgrid with energy saving. *Electr. Power Syst. Res.* **214**, 108792. https://doi.org/10.1016/j.epsr.2022.108792 (2023).
48. Nodehi, M., Zafari, A. & Radmehr, M. A new energy management scheme for electric vehicles microgrids concerning demand response and reduced emission. *Sustain. Energy, Grids Netw.* **32**, 100927. https://doi.org/10.1016/j.segan.2022.100927 (2022).
49. Eghbali, N., Hakimi, S. M., Hasankhani, A., Derakhshan, G. & Abdi, B. A scenario-based stochastic model for day-ahead energy management of a multi-carrier microgrid considering uncertainty of electric vehicles. *J. Energy Storage* **52**, 104843. https://doi.org/10.1016/j.est.2022.104843 (2022).
50. Taghizadegan, N., Cheshmeh Khavar, S., Abdolahi, A., Arasteh, F. & Ghoreyshi, R. Dominated GSO algorithm for optimal scheduling of renewable microgrids with penetration of electric vehicles and energy storages considering DRP. *Int. J. Ambient Energy* **43**, 6380–6391. https://doi.org/10.1080/01430750.2021.2019110 (2022).
51. Amrutha Raju, B. & Sandeep, V. A chance constraint microgrid energy management with phase balancing using electric vehicle demand aggregation. *Energy Sources Part A Recover Util. Environ. Eff.* **45**, 111–139. https://doi.org/10.1080/15567036.2022.2164812 (2023).
52. Arunkumar, A. P. *et al.* An extensive review on energy management system for microgrids. *Energy Sources Part A Recover. Util. Environ. Eff.* **44**, 4203–4228. https://doi.org/10.1080/15567036.2022.2075059 (2022).
53. Rajagopalan, A. *et al.* Multi-objective optimal scheduling of a microgrid using oppositional gradient-based grey wolf optimizer. *Energies* **15**, 9024. https://doi.org/10.3390/en15239024 (2022).
54. Kumar, R. P. & Karthikeyan, G. A multi-objective optimization solution for distributed generation energy management in microgrids with hybrid energy sources and battery storage system. *J. Energy Storage* **75**, 109702. https://doi.org/10.1016/j.est.2023.109702 (2024).
55. Ghasemi, E., Ranjbaran, A. & Pourhossein, J. Designing multi-objective electric and thermal energy management system of microgrid in the presence of controllable loads and electric vehicles. *Electr. Eng.* **106**, 1519–1532. https://doi.org/10.1007/s00202-023-01823-5 (2024).
56. Li, M., Aksoy, M. & Samad, S. Optimal energy management and scheduling of a microgrid with integrated electric vehicles and cost minimization. *Soft Comput.* **28**, 2015–2034. https://doi.org/10.1007/s00500-023-09168-8 (2024).
57. Wang, Y., Wang, B. & Farjam, H. Multi-objective scheduling and optimization for smart energy systems with energy hubs and microgrids. *Eng. Sci. Technol. Int. J.* **51**, 101649. https://doi.org/10.1016/j.jestch.2024.101649 (2024).
58. Huang, A., Mao, Y., Chen, X., Xu, Y. & Wu, S. A multi-timescale energy scheduling model for microgrid embedded with differentiated electric vehicle charging management strategies. *Sustain. Cities Soc.* **101**, 105123. https://doi.org/10.1016/j.scs.2023.105123 (2024).
59. Seyednouri, S. R. *et al.* Day-ahead scheduling of multi-energy microgrids based on a stochastic multi-objective optimization model. *Energies* **16**, 1802. https://doi.org/10.3390/en16041802 (2023).
60. Hai, T., Zhou, J., Rezvani, A., Le, B. N. & Oikawa, H. Optimal energy management strategy for a renewable based microgrid with electric vehicles and demand response program. *Electr. Power Syst. Res.* **221**, 109370. https://doi.org/10.1016/j.epsr.2023.109370 (2023).

61. Ahmed, I., Rehan, M., Basit, A., Tufail, M. & Hong, K.-S. A dynamic optimal scheduling strategy for multi-charging scenarios of plug-in-electric vehicles over a smart grid. *IEEE Access* **11**, 28992–29008. https://doi.org/10.1109/ACCESS.2023.3258859 (2023).
62. Cavus, M., Allahham, A., Adhikari, K., Zangiabadi, M. & Giaouris, D. Energy management of grid-connected microgrids using an optimal systems approach. *IEEE Access* **11**, 9907–9919. https://doi.org/10.1109/ACCESS.2023.3239135 (2023).
63. Ankar, S. J. & Pinkymol, K. P. Optimal sizing and energy management of electric vehicle hybrid energy storage systems with multi-objective optimization criterion. *IEEE Trans. Veh. Technol.* https://doi.org/10.1109/TVT.2024.3372137 (2024).
64. Yang, M., Cui, Y. & Wang, J. Multi-Objective optimal scheduling of island microgrids considering the uncertainty of renewable energy output. *Int. J. Electr. Power Energy Syst.* **144**, 108619. https://doi.org/10.1016/j.ijepes.2022.108619 (2023).
65. Karimi, H., Jadid, S. & Hasanzadeh, S. Optimal-sustainable multi-energy management of microgrid systems considering integration of renewable energy resources: A multi-layer four-objective optimization. *Sustain. Prod. Consum.* **36**, 126–138. https://doi.org/10.1016/j.spc.2022.12.025 (2023).
66. Asaad, A. *et al.* Multi-objective optimal planning of EV charging stations and renewable energy resources for smart microgrids. *Energy Sci. Eng.* **11**, 1202–1218. https://doi.org/10.1002/ese3.1385 (2023).
67. Huang, Y. *et al.* Multi-objective particle swarm optimization for optimal scheduling of household microgrids. *Front. Energy Res.* **11**, 1354869. https://doi.org/10.3389/fenrg.2023.1354869 (2024).
68. Guan, Z. *et al.* Multi-objective optimal scheduling of microgrids based on improved particle swarm algorithm. *Energies* **17**, 1760. https://doi.org/10.3390/en17071760 (2024).
69. Wu, Z., Zou, Y., Zheng, F. & Liang, N. Research on optimal scheduling strategy of microgrid considering electric vehicle access. *Symmetry (Basel).* **15**, 1993. https://doi.org/10.3390/sym15111993 (2023).
70. Yu, Z. *et al.* Grid scheduling strategy considering electric vehicles participating in multi-microgrid interaction. *J. Electr. Eng. Technol.* **18**, 1557–1572. https://doi.org/10.1007/s42835-022-01294-x (2023).
71. Abid, M. S. *et al.* A novel multi-objective optimization based multi-agent deep reinforcement learning approach for microgrid resources planning. *Appl. Energy* **353**, 122029. https://doi.org/10.1016/j.apenergy.2023.122029 (2024).
72. Hao, J., Huang, T., Xu, Q. & Sun, Y. Robust optimal scheduling of microgrid with electric vehicles based on Stackelberg game. *Sustainability* **15**, 16682. https://doi.org/10.3390/su152416682 (2023).
73. Cui, F., Lin, X., Zhang, R. & Yang, Q. Multi-objective optimal scheduling of charging stations based on deep reinforcement learning. *Front. Energy Res.* **10**, 1042882. https://doi.org/10.3389/fenrg.2022.1042882 (2023).
74. Song, J., Mingotti, A., Zhang, J., Peretto, L. & Wen, H. Fast iterative-interpolated DFT phasor estimator considering out-of-band interference. *IEEE Trans. Instrum. Meas.* **71**, 1–14. https://doi.org/10.1109/TIM.2022.3203459 (2022).
75. Talatahari, S., Azizi, M., Tolouei, M., Talatahari, B. & Sareh, P. Crystal structure algorithm (CryStAl): A metaheuristic optimization method. *IEEE Access* **9**, 71244–71261. https://doi.org/10.1109/ACCESS.2021.3079161 (2021).
76. Tavazoei, M. S. & Haeri, M. Comparison of different one-dimensional maps as chaotic search pattern in chaos optimization algorithms. *Appl. Math. Comput.* **187**, 1076–1085. https://doi.org/10.1016/j.amc.2006.09.087 (2007).
77. Karaboga, D. & Akay, B. A comparative study of artificial bee colony algorithm. *Appl. Math. Comput.* **214**, 108–132. https://doi.org/10.1016/j.amc.2009.03.090 (2009).
78. Fathy, A. Bald eagle search optimizer-based energy management strategy for microgrid with renewable sources and electric vehicles. *Appl. Energy* **334**, 120688. https://doi.org/10.1016/j.apenergy.2023.120688 (2023).
79. Zhang, X., Wang, Z. & Lu, Z. Multi-objective load dispatch for microgrid with electric vehicles using modified gravitational search and particle swarm optimization algorithm. *Appl. Energy* **306**, 118018. https://doi.org/10.1016/j.apenergy.2021.118018 (2022).
80. Liang, J. *et al.* An energy-oriented torque-vector control framework for distributed drive electric vehicles. *IEEE Trans. Transp. Electrif.* **9**, 4014–4031. https://doi.org/10.1109/TTE.2022.3231933 (2023).
81. Zhang, X., Wang, Y., Yuan, X., Shen, Y. & Lu, Z. Adaptive dynamic surface control with disturbance observers for battery/supercapacitor-based hybrid energy sources in electric vehicles. *IEEE Trans. Transp. Electrif.* **9**, 5165–5181. https://doi.org/10.1109/TTE.2022.3194034 (2023).
82. Zhang, X., Lu, Z., Yuan, X., Wang, Y. & Shen, X. L2-gain adaptive robust control for hybrid energy storage system in electric vehicles. *IEEE Trans. Power Electron.* **36**, 7319–7332. https://doi.org/10.1109/TPEL.2020.3041653 (2021).
83. Zhang, X. *et al.* Voltage and frequency stabilization control strategy of virtual synchronous generator based on small signal model. *Energy Rep.* **9**, 583–590. https://doi.org/10.1016/j.egyr.2023.03.071 (2023).
84. Yan, C., Zou, Y., Wu, Z. & Maleki, A. Effect of various design configurations and operating conditions for optimization of a wind/solar/hydrogen/fuel cell hybrid microgrid system by a bio-inspired algorithm. *Int. J. Hydrogen Energy* **60**, 378–391. https://doi.org/10.1016/j.ijhydene.2024.02.004 (2024).
85. Zheng, S., Hai, Q., Zhou, X. & Stanford, R. J. A novel multi-generation system for sustainable power, heating, cooling, freshwater, and methane production: Thermodynamic, economic, and environmental analysis. *Energy* **290**, 130084. https://doi.org/10.1016/j.energy.2023.130084 (2024).
86. Li, S., Zhao, X., Liang, W., Hossain, M. T. & Zhang, Z. A fast and accurate calculation method of line breaking power flow based on taylor expansion. *Front. Energy Res.* **10**, 943946. https://doi.org/10.3389/fenrg.2022.943946 (2022).
87. Fang, Z. *et al.* Enhancing robust driver assistance control in distributed drive electric vehicles through integrated AFS and DYC technology. *IEEE Trans. Intell. Veh.* https://doi.org/10.1109/TIV.2024.3368050 (2024).
88. Ghaedi, A., Dehnavi, S. D. & Fotoohabadi, H. Probabilistic scheduling of smart electric grids considering plug-in hybrid electric vehicles. *J. Intell. Fuzzy Syst.* **31**, 1329–1340. https://doi.org/10.3233/IFS-162199 (2016).
89. Song, J., Mingotti, A., Zhang, J., Peretto, L. & Wen, H. Accurate damping factor and frequency estimation for damped real-valued sinusoidal signals. *IEEE Trans. Instrum. Meas.* **71**, 1–4. https://doi.org/10.1109/TIM.2022.3220300 (2022).
90. Qian, K., Zhou, C., Allan, M. & Yuan, Y. Modeling of load demand due to EV battery charging in distribution systems. *IEEE Trans. Power Syst.* **26**, 802–810. https://doi.org/10.1109/TPWRS.2010.2057456 (2011).
91. Fathy, A. & Abdelaziz, A. Y. Single and multi-objective operation management of micro-grid using krill herd optimization and ant lion optimizer algorithms. *Int. J. Energy Environ. Eng.* **9**, 257–271. https://doi.org/10.1007/s40095-018-0266-8 (2018).
92. Aghajani, G. & Ghadimi, N. Multi-objective energy management in a micro-grid. *Energy Rep.* **4**, 218–225. https://doi.org/10.1016/j.egyr.2017.10.002 (2018).
93. Aghajani, G. R., Shayanfar, H. A. & Shayeghi, H. Presenting a multi-objective generation scheduling model for pricing demand response rate in micro-grid energy management. *Energy Convers. Manag.* **106**, 308–321. https://doi.org/10.1016/j.enconman.2015.08.059 (2015).
94. Fang, Z. *et al.* Authority allocation strategy for shared steering control considering human-machine mutual trust level. *IEEE Trans. Intell. Veh.* **9**, 2002–2015. https://doi.org/10.1109/TIV.2023.3300152 (2024).
95. Liang, J. *et al.* A direct yaw moment control framework through robust T-S fuzzy approach considering vehicle stability margin. *IEEE/ASME Trans. Mechatron.* **29**, 166–178. https://doi.org/10.1109/TMECH.2023.3274689 (2024).
96. Li, Z. *et al.* A LiDAR-OpenStreetMap matching method for vehicle global position initialization based on boundary directional feature extraction. *IEEE Trans. Intell. Veh.* https://doi.org/10.1109/TIV.2024.3393229 (2024).
97. Bai, X., He, Y. & Xu, M. Low-thrust reconfiguration strategy and optimization for formation flying using Jordan normal form. *IEEE Trans. Aerosp. Electron. Syst.* **57**, 3279–3295. https://doi.org/10.1109/TAES.2021.3074204 (2021).

98. Venkatesh, P., Gnanadass, R. & Padhy, N. P. Comparison and application of evolutionary programming techniques to combined economic emission dispatch with line flow constraints. *IEEE Trans. Power Syst.* **18**, 688–697. https://doi.org/10.1109/TPWRS.2003.811008 (2003).
99. Liang, J. *et al.* ETS-based human-machine robust shared control design considering the network delays. *IEEE Trans. Autom. Sci. Eng.* https://doi.org/10.1109/TASE.2024.3383094 (2024).
100. Chen, J. *et al.* Geometrical state-plane-based synchronous rectification scheme for LLC converter in EVs. *IEEE Trans. Transp. Electrif.* https://doi.org/10.1109/TTE.2024.3383208 (2024).
101. Karthik, N., Parvathy, A. K., Arul, R. & Padmanathan, K. A new heuristic algorithm for economic load dispatch incorporating wind power. In *Artificial Intelligence and Evolutionary Computations in Engineering Systems* 47–65 (Springer, 2022). https://doi.org/10.1007/978-981-16-2674-6_5.
102. Karthik, N., Rajagopalan, A., Prakash, V. R., Montoya, O. D., Sowmmiya, U. & Kanimozhi, R. (2023). Environmental economic load dispatch considering demand response using a new heuristic optimization algorithm. In *AI Techniques for Renewable Source Integration and Battery Charging Methods in Electric Vehicle Applications*, pp. 220-242. https://doi.org/10.4018/978-1-6684-8816-4.ch013
103. Nagarajan, K., Rajagopalan, A., Selvaraj, P., Ravi, H. K. & Kareem, I. A. Demand response-integrated economic emission dispatch using improved remora optimization algorithm. In *AI Approaches to Smart Sustain and Power Systems* (ed. Global, I. G. I.) 120–140 (2024). https://doi.org/10.4018/979-8-3693-1586-6.ch007.
104. Biswas, P. P., Suganthan, P. N. & Amaratunga, G. A. Optimal power flow solutions incorporating stochastic wind and solar power. *Energy Convers. Manag.* **148**, 1194–1207 (2017).
105. Abdullah, M., Javaid, N., Chand, A., Khan, Z. A., Waqas, M. & Abbas, Z. Multi-objective optimal power flow using improved multi-objective multi-verse algorithm. In *Web, Artificial Intelligence and Network Applications: Proceedings of the Workshops of the 33rd International Conference on Advanced Information Networking and Applications (WAINA-2019)*, Vol. 33 (pp. 1071–1083, Springer International Publishing, 2019).
106. Abdullah, M., Javaid, N., Khan, I. U., Khan, Z. A., Chand, A. & Ahmad, N. Optimal power flow with uncertain renewable energy sources using flower pollination algorithm. In *Advanced Information Networking and Applications: Proceedings of the 33rd International Conference on Advanced Information Networking and Applications (AINA-2019)*, Vol. 33 (pp. 95–107, Springer International Publishing, 2020).
107. Biswas, P. P., Suganthan, P. N., Qu, B. Y. & Amaratunga, G. A. Multiobjective economic-environmental power dispatch with stochastic wind-solar-small hydro power. *Energy* **150**, 1039–1057 (2018).
108. Karthik, N. *et al.* Multi-objective optimal power flow using a new heuristic optimization algorithm with the incorporation of renewable energy sources. *Int. J. Energy Environ. Eng.* https://doi.org/10.1007/s40095-021-00397-x (2021).
109. Bai, X., Xu, M., Li, Q. & Yu, L. Trajectory-battery integrated design and its application to orbital maneuvers with electric pump-fed engines. *Adv. Sp. Res.* **70**, 825–841. https://doi.org/10.1016/j.asr.2022.05.014 (2022).
110. Rong, Y. *et al.* Du-bus: A realtime bus waiting time estimation system based on multi-source data. *IEEE Trans. Intell. Transp. Syst.* **23**, 24524–24539. https://doi.org/10.1109/TITS.2022.3210170 (2022).
111. Oubelaid, A. *et al.* New coordinated drive mode switching strategy for distributed drive electric vehicles with energy storage system. *Sci. Rep.* **14**, 6448. https://doi.org/10.1038/s41598-024-56209-9 (2024).
112. Punyavathi, R. *et al.* Sustainable power management in light electric vehicles with hybrid energy storage and machine learning control. *Sci. Rep.* **14**, 5661. https://doi.org/10.1038/s41598-024-55988-5 (2024).
113. Naoussi, S. R. D. *et al.* Enhancing MPPT performance for partially shaded photovoltaic arrays through backstepping control with Genetic algorithm-optimized gains. *Sci. Rep.* **14**, 3334. https://doi.org/10.1038/s41598-024-53721-w (2024).
114. Nagarajan, K. *et al.* Optimizing dynamic economic dispatch through an enhanced Cheetah-inspired algorithm for integrated renewable energy and demand-side management. *Sci. Rep.* **14**, 3091. https://doi.org/10.1038/s41598-024-53688-8 (2024).
115. Fathy, A., Rezk, H., Ferahtia, S., Ghoniem, R. M. & Alkanhel, R. An efficient honey badger algorithm for scheduling the microgrid energy management. *Energy Rep.* **9**, 2058–2074. https://doi.org/10.1016/j.egyr.2023.01.028 (2023).

Acknowledgements

This article has been produced with the financial support of the European Union under the REFRESH—Research Excellence For Region Sustainability and High-tech Industries project Number CZ.10.03.01/00/22_003/0000048 via the Operational Programme Just Transition and paper was supported by the following project TN02000025 National Centre for Energy II. The authors also wish to thank the Hindustan Institute of Technology & Science, Chennai, India, Vellore Institute of Technology, Chennai, India and Graphic Era (Deemed to be University), Dehradun, India for their all support and encouragement to carry out this work.

Author contributions

Karthik Nagarajan, Arul Rajagopalan : Conceptualization, Methodology, Software, Visualization, Investigation, Writing–Original draft preparation. Sowmmiya Uthayakumar: Data curation, Validation, Supervision, Resources, Writing–Review & Editing. Mohit Bajaj, Lukas Prokop, Vojtech Blazek: Project administration, Supervision, Resources, Writing–Review & Editing.

Competing interests

The authors declare no competing interests.

Additional information

Correspondence and requests for materials should be addressed to A.R. or M.B.

Reprints and permissions information is available at www.nature.com/reprints.

Publisher's note Springer Nature remains neutral with regard to jurisdictional claims in published maps and institutional affiliations.

Open Access This article is licensed under a Creative Commons Attribution 4.0 International License, which permits use, sharing, adaptation, distribution and reproduction in any medium or format, as long as you give appropriate credit to the original author(s) and the source, provide a link to the Creative Commons licence, and indicate if changes were made. The images or other third party material in this article are included in the article's Creative Commons licence, unless indicated otherwise in a credit line to the material. If material is not included in the article's Creative Commons licence and your intended use is not permitted by statutory regulation or exceeds the permitted use, you will need to obtain permission directly from the copyright holder. To view a copy of this licence, visit http://creativecommons.org/licenses/by/4.0/.

© The Author(s) 2024